Multistability and gluing bifurcation to butterflies in coupled networks with non-monotonic feedback

2009 Nonlinearity 22 1383

(http://iopscience.iop.org/0951-7715/22/6/007)

IOP PUBLISHING NONLINEARITY

Nonlinearity **22** (2009) 1383–1412 doi:10.1088/0951-7715/22/6/007

Multistability and gluing bifurcation to butterflies in coupled networks with non-monotonic feedback

Jianfu Ma[1] **and Jianhong Wu**[2]

[1] Department of Mathematics, University of Houston, Houston TX 77204-3008, USA
[2] Laboratory for Industrial and Applied Mathematics, Department of Mathematics and Statistics, York University, Toronto, Ontario M3J 1P3, Canada

E-mail: majf@math.uh.edu and wujh@mathstat.yorku.ca

Received 19 October 2008, in final form 13 April 2009
Published 7 May 2009
Online at stacks.iop.org/Non/22/1383

Recommended by J A Glazier

Abstract

Neural networks with a non-monotonic activation function have been proposed to increase their capacity for memory storage and retrieval, but there is still a lack of rigorous mathematical analysis and detailed discussions of the impact of time lag. Here we consider a two-neuron recurrent network. We first show how supercritical pitchfork bifurcations and a saddle-node bifurcation lead to the coexistence of multiple stable equilibria (multistability) in the instantaneous updating network. We then study the effect of time delay on the local stability of these equilibria and show that four equilibria lose their stability at a certain critical value of time delay, and Hopf bifurcations of these equilibria occur simultaneously, leading to multiple coexisting periodic orbits. We apply centre manifold theory and normal form theory to determine the direction of these Hopf bifurcations and the stability of bifurcated periodic orbits. Numerical simulations show very interesting global patterns of periodic solutions as the time delay is varied. In particular, we observe that these four periodic solutions are glued together along the stable and unstable manifolds of saddle points to develop a butterfly structure through a complicated process of gluing bifurcations of periodic solutions.

Mathematics Subject Classification: 34K13, 34K17, 34K18, 37G15, 37G35, 92B20

1. Introduction

Autocorrelation model for associative memory, a major neural network architecture, was proposed in the early 1970s (see [1, 31, 41]) and has been one of the inspirations for the rapid development in the theory and applications of both biological and artificial neural networks

(see [2, 40, 55]). Hopfield [27] showed that a simple discrete nonlinear dynamical system describing the performance of an additive model with discrete updating can exhibit associative recall of stored binary patterns through collective computing. Cohen and Grossberg [16] and Hopfield [28] also obtained powerful convergence results for general additive neural network models with symmetric synaptic connection matrices of instantaneous feedbacks described by a system of ordinary differential equations. Their results demonstrate the significance of understanding the structure and stability of equilibria and their domains of attraction in connection with neural network applications to associative memory.

Time delay, arising from axonal conduction time, distances of interneurons and finite switching speeds of amplifiers [20, 21], seems to provide an efficient mechanism for neural networks to store and retrieve periodic patterns [20, 21, 38] despite the undesirable nonlinear oscillations in hardware implementation first observed by Marcus and Westervelt [36]. These delay-induced or delay-enhanced spatiotemporal pattern formation, storage and retrieval have been intensively studied in [3, 4, 25, 26, 47, 54]. In particular, systems of two coupled delay differential equations describing the information processing of a network of two neurons with delayed feedback are considered in [10–15], where the issues of multiple periodic orbits, the detailed description of the domains of attraction of periodic solutions and the structure of the global attractor are addressed.

The coexistence of multiple stable patterns such as equilibria and periodic orbits (multistability) in a neural network is the basis for associative memory storage and retrieval [20, 27, 28, 35, 38, 40, 52, 53]. Stable equilibria have been proposed as a robust representation of prototype vectors in associative memory [28, 29]. Indeed, a great deal of work has focused on the question of how to constrain the weights in a recurrent network so that the network exhibits only stable states [30, 46, 50, 56]. Stable periodic orbits play an important role in coding and transmitting information of memories as temporally patterned spike trains in the nervous system [9, 20, 21, 35, 53]. There are basically three ways in which a neuron model can switch from a stable steady state to a periodic orbit: (a) Hopf bifurcation, (b) saddle-node bifurcation on a limit cycle and (c) homoclinic bifurcation. Time delays are commonly associated with oscillations created by a Hopf bifurcation.

On the other hand, saddle steady states were suggested to play an important role in working memories operating in non-stationary environments where both long-term maintenance and quick transitions are desirable [37, 42]. Saddle points were also found to be part of a mechanism by which recurrent networks induce non-stable representations of large cycles in finite state machines [49].

The aforementioned stable equilibria, saddle points and periodic orbits provide stretching, folding and contraction of the semiflows of dynamical systems at the local level. Homoclinic orbits characterize a recurrent mechanism and heteroclinic orbits provide transition routes for global folding in the phase space. Their crucial roles in the mechanism originating chaos in dynamical systems are now widely recognized [19, 43, 48]. The theory of homoclinic and heteroclinic orbits is well developed for ODE models [19, 32, 51]. In contrast, homoclinic and heteroclinic orbits in DDEs have not been so well studied, except [33, 34]. In particular, to our knowledge, the analysis of the effect of the homoclinic and heteroclinic orbits on associative memory storage and retrieval is still missing.

Potential applications require the dynamical system describing the computational performance of the network to have as many stable equilibria or stable periodic orbits as possible. Unfortunately, most of the aforementioned neural network architectures present major problems as an associative memory device due to the low memory capacity [40]. Motivated by this observation, Morita *et al* [39, 40] and Yoshizawa *et al* [55] introduced a non-monotonic activation function, and showed that the performance of the associative memory

can be remarkably improved by using a non-monotonic activation function. This improvement of the network's capacity for memory storage and retrieval seems to have great potential for artificial neural network applications. However, as Morita concluded in [39], 'there still remain some important problems such as mathematical analysis and biological relevance; we should further study improved dynamics for developing information processing by neural networks.'

A full mathematical analysis of the dynamics of such a general network may still be remote until a detailed case study can be attempted, not to mention the additional difficulty by incorporating time delay. In this paper, we focus on the following simplified recurrent network of two identical neurons coupled via a non-monotonic activation function with a discrete time delay

$$\begin{aligned} x'(t) &= -\alpha x + Wf(y(t-\tau)), \\ y'(t) &= -\alpha y + Wf(x(t-\tau)), \end{aligned} \tag{1.1}$$

where the activation function $f : \mathbb{R} \to \mathbb{R}$ is given by

$$f(x) = \frac{1-\exp[-\beta_1 x]}{1+\exp[-\beta_1 x]} \times \frac{1+k\exp[\beta_2(|x|-h)]}{1+\exp[\beta_2(|x|-h)]}. \tag{1.2}$$

Here x, y represent the activations of neurons, $\alpha > 0$ is the ratio of the capacitance to the resistance, W is the synaptic connection strength, $\tau \geqslant 0$ is the time delay, β_1 and β_2 are positive constants and h, k are parameters. See the graph of such a function in figure 1.

There is a considerable amount of literature on two-neuron recurrent networks [7, 8, 22, 35, 47]. These previous studies show that two-neuron recurrent networks display similar complex dynamic behaviours as larger networks and many techniques developed to deal with two-neuron networks can carry over to large size networks. Moreover, two-neuron networks are sometimes thought of as systems of two modules, where each module represents the mean activity of spatially localized neural populations [5, 50].

The purposes of this paper are to provide a rigorous mathematical analysis of the mechanism for system (1.1) to generate a large number of coexisting stable patterns including equilibria and periodic orbits, and to understand local bifurcation and global continuation of periodic solutions for system (1.1). We shall show that within a certain parameter range, model (1.1) with the instantaneous feedback possesses multiple symmetric steady states, including six stable equilibria, five unstable equilibria (saddle) and six heteroclinic orbits connecting these steady states. This coexistence of multiple stable equilibria in the instantaneous updating network occurs through the mechanisms of supercritical pitchfork bifurcations and saddle-node bifurcations.

Time delay has a profound impact on the global dynamics of system (1.1). In particular, increasing time delay to a critical value, the occurrence of Hopf bifurcations of the four equilibria results in four periodic orbits simultaneously, which have a reflection symmetry about the heteroclinic orbits, which are segments in the lines $y = x$ and $y = -x$ in the projected (x, y)-plane of the phase space. As the delay increases, the corresponding periodic orbits with such a reflection symmetry evolve in a similar manner and approach the separatrix of the saddle points. A butterfly configuration arises from a gluing bifurcation in which the saddle points experience homoclinicity on both sides of their stable manifolds simultaneously. In the gluing process, two homoclinic orbits are generated on opposite sides of the stable manifold of the saddle-focus point and the periods of the periodic orbits increase monotonically towards infinity as the time delay reaches the bifurcation value. With the reflection symmetry, the gluing bifurcation has codimension one since only one parameter, the delay, is required to control the homoclinic connection of periodic orbits.

Gluing together two periodic orbits is a special process of global continuation during which two periodic orbits living on the opposite sides of a saddle separatrix are destroyed and a new attractor is created occupying the loci in the phase space of the previous ones. The gluing bifurcation seems to have first been introduced by Coullet *et al* [17] in 1984 and has been studied in the literature for two-dimensional and three-dimensional dynamical systems [6, 17, 24, 44]. In particular, Borisyuk *et al* [6] found a torus gluing bifurcation in two coupled neural oscillators with connections between mutual excitatory neural populations. In a two-dimensional system, the gluing process is simple, where two limit cycles are glued together to a two-lobed limit cycle. In a three-dimensional system, the possibility of different homoclinic connections increases indefinitely and a large variety of hybrid periodic orbits may be created. In a three-dimensional system with a reflection symmetry, a gluing bifurcation can occur in one of three configurations: figure-of-eight, butterfly configuration and spiral configuration (a pair of orbits homoclinic to a saddle-focus).

Here, we observe a gluing bifurcation which possesses both spiral configuration and butterfly configuration in the delay differential system (1.1) as the time delay increases passing through certain values. We also note gluing processes of periodic solutions which cross the stable manifolds of the saddle points in the projected (x, y)-plane several times. Furthermore, we find an interesting bifurcation process, called an *inverse gluing bifurcation*, where a large periodic orbit approaches a saddle point along both sides of the saddle separatrix to generate two homoclinic orbits (at the inverse gluing bifurcation point), and then two smaller periodic orbits emerge near the homoclinic orbits when the delay is further increased.

The paper is organized as follows. In section 2, we normalize our model (1.1) and discuss some basic properties of the non-monotonic activation function (1.2). In section 3, we study the normalized model with the instantaneous feedback ($\tau = 0$) to locate all possible equilibria in the parameter space, to describe the local stability of these equilibria and to investigate pitchfork and saddle-node bifurcations which result in multistability in the form of stable equilibria. In sections 4 and 5, we analyse the effect of time delay on the stability of equilibria, examine Hopf bifurcations of these equilibria, and apply centre manifold theory and normal form theory to study the direction of the Hopf bifurcations and the stability of bifurcated periodic orbits. In section 6, we investigate the global dynamical behaviours of system (1.1) and illustrate the butterfly phenomena via a sequence of gluing and inverse gluing bifurcations. In the final section, we discuss some implications of our results in the context of associative memory.

2. Preliminaries

We first re-scale system (1.1), using the following variables: $\bar{x}(t) = x(t/W)$, $\bar{y}(t) = y(t/W)$, $\bar{\alpha} = \alpha/W$, $\bar{\tau} = W\tau$. Dropping the bar on x, y, α and τ without any notational confusion, we obtain the following system:

$$\begin{aligned} x'(t) &= -\alpha x + f(y(t-\tau)), \\ y'(t) &= -\alpha y + f(x(t-\tau)). \end{aligned} \tag{2.3}$$

In what follows, we shall focus on the above normalized model to discuss the long-term dynamical behaviours of system (1.1). Equilibrium solutions of system (2.3) must satisfy

$$\alpha x = f(y), \qquad \alpha y = f(x). \tag{2.4}$$

We rewrite $f(x) = \sigma_1(x)\sigma_2(x)$ where

$$\sigma_1(x) = \frac{1 - \exp[-\beta_1 x]}{1 + \exp[-\beta_1 x]}, \qquad \sigma_2(x) = \frac{1 + k\exp[\beta_2(|x| - h)]}{1 + \exp[\beta_2(|x| - h)]}.$$

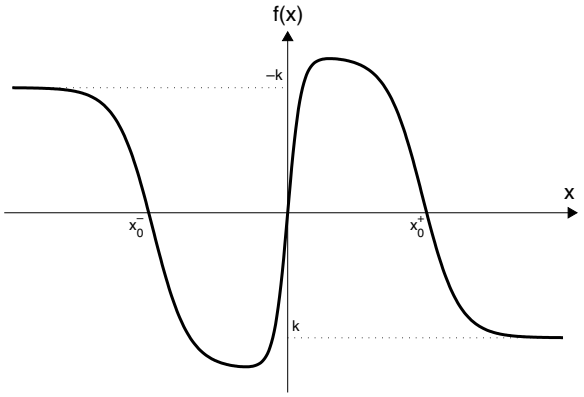

Figure 1. A nonmonotonic activation function $f(x)$ when $k < 0$, $h > 0$, $\beta_1, \beta_2 > 0$.

Function $\sigma_1 : \mathbb{R} \to \mathbb{R}$ is a sigmoid function which satisfies $\sigma_1(0) = 0$, $0 \leqslant \sigma_1 < 1$, $\sigma_1 \in C^\infty(\mathbb{R})$ and

$$\sigma_1(-x) = \frac{1 - \exp[\beta_1 x]}{1 + \exp[\beta_1 x]} = -\frac{1 - \exp[-\beta_1 x]}{1 + \exp[-\beta_1 x]} = -\sigma_1(x).$$

The origin $(0, 0)$ satisfies equation (2.4), hence it is always an equilibrium. On the other hand, function $\sigma_2 : \mathbb{R} \to \mathbb{R}$ is an even function, $\sigma_2 \in C^\infty(\mathbb{R}\backslash\{0\})$. This function has no zero root if $k \geqslant 0$, and has two zeros if $k < 0$: x_0^+ and x_0^- given by

$$x_0^+ = h + \frac{\log(-1/k)}{\beta_2}, \qquad x_0^- = -h - \frac{\log(-1/k)}{\beta_2}.$$

The derivatives of $\sigma_1(x)$ and $\sigma_2(x)$ are given by

$$\sigma_1'(x) = \frac{1}{2}\beta_1(1 + \sigma_1)(1 - \sigma_1),$$

$$\sigma_2'(x) = \operatorname{sgn}(x)\frac{\beta_2(\sigma_2 - 1)(k - \sigma_2)}{k - 1} \qquad \text{for } x \neq 0,$$

where $\operatorname{sgn}(x)$ is the sign of x. Hence, $\sigma_1'(x)$ is an even function and $\sigma_2'(x)$ is an odd function.

We list some properties of f, for the sake of later usage in discussing the stability of equilibria and computing the centre manifold when a Hopf bifurcation occurs:

(i) $\lim_{x\to+\infty} f(x) = k$ and $\lim_{x\to-\infty} f(x) = -k$;
(ii) For $k < 0$, $f(x) = 0$ has three roots: $x_0 = 0, x_0^+, x_0^-$;
(iii) f is an odd function, f' is a continuous even function on $x \in \mathbb{R}$ and

$$f'(x) = \begin{cases} \dfrac{1}{2}\beta_1(1 + \sigma_1)(1 - \sigma_1)\sigma_2 + \operatorname{sgn}(x)\dfrac{\beta_2\sigma_1(\sigma_2 - 1)(k - \sigma_2)}{k - 1} & \text{if } x \neq 0, \\ \dfrac{1}{2}\beta_1\dfrac{1 + k\exp[-\beta_2 h]}{1 + \exp[-\beta_2 h]} & \text{if } x = 0; \end{cases} \tag{2.5}$$

(iv) $f \in C^\infty(\mathbb{R}\backslash\{0\})$;
(v) If $k < 0$, there exist $x_{\mathrm{M}}^- \in (x_0^-, 0)$ and $x_{\mathrm{M}}^+ \in (0, x_0^+)$ such that $f'(x_{\mathrm{M}}^-) = f'(x_{\mathrm{M}}^+) = 0$.

Figure 1 illustrates the shape of a non-monotonic function f when $\beta_1, \beta_2 > 0$, $k < 0$ and $h > 0$.

Lemma 2.1.

(i) $(\tilde{x}, \tilde{y}) = (0, 0)$ *is an equilibrium;*
(ii) If $(\tilde{x}, \tilde{y})$ *is an equilibrium, then so is* $(\tilde{y}, \tilde{x})$*;*
(iii) If $(\tilde{x}, \tilde{y})$ *is an equilibrium, then so is* $(-\tilde{x}, -\tilde{y})$.

Equilibria of (2.3) coincide with equilibria of the two-dimensional system $x'(t) = -\alpha x + f(y)$, $y'(t) = -\alpha y + f(x)$. Therefore, in our discussion about the structure of equilibria, we can think of the phase space as (x, y)-plane, although the phase space for (2.3) is infinitely dimensional. Lemma 2.1(iii) suggests that equilibria of system (2.3) are symmetric with respect to the origin in the phase space (x, y)-plane. Furthermore, two symmetric equilibria at $(\tilde{x}, \tilde{y})$ and $(-\tilde{x}, -\tilde{y})$ have the same stability since the derivative of f is an even function (the property (iii) of function f). Hence, we only need to focus on the equilibria with $\tilde{x} \geqslant 0$ (or $\tilde{x} \leqslant 0$), i.e. in the first and fourth quadrants (or, the second and third quadrants). Lemma 2.1(ii) suggests that equilibria of system (2.3) are symmetric about the line $y = x$. With such a symmetry, we only need to focus on the equilibria with $\tilde{y} \geqslant |\tilde{x}|$ (or $\tilde{y} \leqslant |\tilde{x}|$). In what follows, we shall focus on the analysis of the existence and stability of equilibria with either $\tilde{y} \geqslant |\tilde{x}|$ or $\tilde{y} < |\tilde{x}|$ in the first and fourth quadrants, but we shall show equilibria in all quadrants in the phase portraits.

3. Multistability with instantaneous feedback ($\tau = 0$)

An equilibrium, $(\tilde{x}, \tilde{y})$, is the intersection of the curves $y = f(x)/\alpha$ and $x = f(y)/\alpha$. The number of equilibria of system (2.3) depends on values of parameters α, β_1, β_2, k, h. For the potential application to associative memory, we wish to have as many equilibria as possible in the five-dimensional parameter space. In this paper, we restrict to the parameter space in which $h > 0$ and $-1 \leqslant k < 0$ as Morita *et al* did in [39].

In this section, we focus on the case when $\tau = 0$. Stability of an equilibrium, $(\tilde{x}, \tilde{y})$, is determined by the linearized system

$$\begin{aligned} x_1'(t) &= -\alpha x_1 + f'(\tilde{y})x_2 = -\alpha x_1 + \tilde{\mu} x_2, \\ x_2'(t) &= -\alpha x_2 + f'(\tilde{x})x_1 = -\alpha x_2 + \mu x_1, \end{aligned} \tag{3.6}$$

where $(x_1(t), x_2(t)) = (x(t) - \tilde{x}, y(t) - \tilde{y})$, $\tilde{\mu} = f'(\tilde{y})$ and $\mu = f'(\tilde{x})$. The characteristic equation is given by

$$\det \begin{pmatrix} \lambda + \alpha & -\tilde{\mu} \\ -\mu & \lambda + \alpha \end{pmatrix} = 0.$$

This gives rise to two eigenvalues

$$\lambda_{1,2} = \begin{cases} -\alpha \pm \sqrt{\mu\tilde{\mu}} & \text{if } \mu\tilde{\mu} \geqslant 0; \\ -\alpha \pm i\sqrt{|\mu\tilde{\mu}|} & \text{if } \mu\tilde{\mu} < 0. \end{cases} \tag{3.7}$$

It is well known that the equilibrium is locally asymptotically stable if both eigenvalues λ_1 and λ_2 have negative real parts, and unstable if one or more of the eigenvalues has a positive real part. Therefore, we have

Theorem 3.1. *If* $\mu\tilde{\mu} < \alpha^2$*, an equilibrium,* $(\tilde{x}, \tilde{y})$*, is locally asymptotically stable; if* $\mu\tilde{\mu} > \alpha^2$*, the equilibrium is unstable. If* $\mu\tilde{\mu} = \alpha^2$*, one eigenvalue is zero, and hence a bifurcation occurs.*

In what follows, we describe in detail the bifurcation process for system (2.3) to exhibit one, three, seven and eleven equilibria, and label these equilibria as $E_1, E_2, \ldots, E_{11}$. Note that the subindex of each equilibrium will be used only to label the equilibrium for ease of reference. We know that system (2.3) always has an equilibrium at origin $(0, 0)$, denoted by $E_1(0, 0)$.

One equilibrium $E_1(0, 0)$. Let $\mu_1 = f'(0)$ be the slope of the curve of $y = f(x)$ at the origin $E_1(0, 0)$. If $0 < \mu_1 < \alpha$, there is only one intersection of the two curves y=$f(x)/\alpha$ and $x = f(y)/\alpha$, and this is the origin $E_1(0, 0)$. By theorem 3.1 with $\mu = \tilde{\mu} = \mu_1$, the equilibrium $E_1(0, 0)$ is asymptotically stable.

When $\mu_1 = \alpha$, the curve $y = f(x)/\alpha$ is tangent to the curve $x = f(y)/\alpha$ at the origin $(0, 0)$ and one eigenvalue of the characteristic equation at the equilibrium E_1 becomes zero. Equilibrium $E_1(0, 0)$ loses its stability and a bifurcation occurs. This is a supercritical pitchfork bifurcation with the stable manifold $W^{\mathrm{s}} = \{(x, y) : y = -x\}$ and a centre manifold $W^{\mathrm{c}} = \{(x, y) : y = x\}$, which results in multistability: the coexistence of two stable equilibria as discussed in the next part (three equilibria). The bifurcation set for $\mu_1 = \alpha$ is given by

$$\frac{1}{2}\beta_1 \frac{1 + k\exp[-\beta_2 h]}{1 + \exp[-\beta_2 h]} = \alpha,$$

that is,

$$\mathrm{e}^{-\beta_2 h} = \frac{\beta_1 - 2\alpha}{2\alpha - \beta_1 k}. \tag{3.8}$$

This means $\beta_1 > 2\alpha$ if $k = -1$; and $2\alpha < \beta_1 \leqslant \frac{4\alpha}{1+k}$ if $-1 < k < 0$. The surface in the parameter space described by (3.8) is the boundary between the regions where (2.3) has one equilibrium or three equilibria.

Three equilibria. When $\mu_1 = f'(0) > \alpha$, equilibrium $E_1(0, 0)$ becomes a saddle (see figure 2(*a*)) since two eigenvalues of the linearization at the equilibrium E_1 have opposite signs. The curves $y = f(x)/\alpha$ and $x = f(y)/\alpha$ have two new intersections symmetric with respect to the origin: $E_2(\tilde{x}_2, \tilde{y}_2)$ and $E_3(-\tilde{x}_2, -\tilde{y}_2)$ with $\tilde{y}_2 = \tilde{x}_2 > 0$. Note that there appear two heteroclinic orbits: one connecting equilibria E_1 and E_2, denoted by E_1E_2, and another one connecting equilibria E_1 and E_3, denoted by E_1E_3.

Let $\mu_2 = f'(\tilde{x}_2)$ be the slope of the curve $y = f(x)$ at E_2. It is clear that $\mu_2 < \alpha$. If $\mu_2 > -\alpha$, then equilibria E_2 and E_3 are both stable by theorem 3.1 with $\mu = \tilde{\mu} = \mu_2$. Figure 2(*a*) shows the phase portrait in this case where (2.3) has three equilibria and two heteroclinic orbits: E_1 (saddle), E_2 and E_3 (stable nodes), E_1E_2 and E_2E_3 (heteroclinic orbits) and the dotted curves are graphs of $y = f(x)/\alpha$ and $x = f(y)/\alpha$.

When $\mu_2 = -\alpha$, the curve $y = f(x)/\alpha$ is tangent to the curve $x = f(y)/\alpha$ at the equilibrium $E_2(\tilde{x}_2, \tilde{y}_2)$. Equilibrium E_2 then loses its stability and a supercritical pitchfork bifurcation occurs, which results in the occurrence of coexisting four stable equilibria. To compute the stable manifold and centre manifold at E_2, we use the Taylor series expansion of the function f at the equilibrium E_2 to obtain the following differential equations

$$\begin{aligned} x_1'(t) &= -\alpha x_1(t) - \alpha x_2(t) + \tfrac{1}{2}f''(\tilde{y}_2)x_2^2(t) + \tfrac{1}{6}f'''(\tilde{y}_2)x_2^3(t) + O(x_2^4), \\ x_2'(t) &= -\alpha x_2(t) - \alpha x_1(t) + \tfrac{1}{2}f''(\tilde{x}_2)x_1^2(t) + \tfrac{1}{6}f'''(\tilde{x}_2)x_1^3(t) + O(x_1^4), \end{aligned} \tag{3.9}$$

where $(x_1(t), x_2(t)) = (x(t) - \tilde{x}_2, y(t) - \tilde{y}_2)$, $f''(\tilde{x}_2) = f''(\tilde{y}_2)$ and $f'''(\tilde{x}_2) = f'''(\tilde{y}_2)$. We compute the centre manifold in the form of

$$x_2 = h(x_1) = ax_1 + bx_1^2 + cx_1^3 + O(x_1^4). \tag{3.10}$$

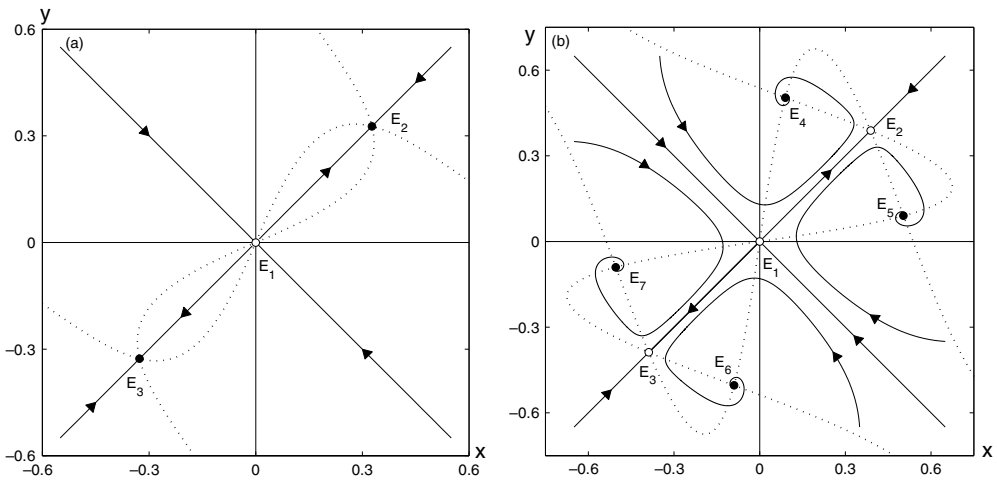

Figure 2. Phase portraits of (2.3) with three equilibria (a) and seven equilibria (b), where the dotted curves are graphs of $y = f(x)/\alpha$ and $x = f(y)/\alpha$.

Differentiating equation (3.10), substituting the second equation into the first equation of (3.9) and comparing the coefficients, we obtain

$$-\alpha - a\alpha = -a\alpha - a^2\alpha,$$
$$\tfrac{1}{2}f''(\tilde{x}_2) - b\alpha = -2b\alpha - 3ab\alpha + \tfrac{1}{2}a^3 f''(\tilde{x}_2),$$
$$\tfrac{1}{6}f'''(\tilde{x}_2) - c\alpha = -3c\alpha - 4ac\alpha + 2a^2 bf''(\tilde{x}_2) + \tfrac{1}{6}a^4 f'''(\tilde{x}_2) - 2b^2\alpha.$$

The first equation gives rise to $a = \pm 1$. When $a = 1$, two other equations yield $b = 0$, $c = 0$; when $a = -1$, $b = \frac{1}{2\alpha}f''(\tilde{x}_2)$, $c = -\frac{1}{4\alpha^2}[f''(\tilde{x}_2)]^2$. We know that the linearized equations of (3.9) have the stable subspace $E^s = \{(x, y) : y = x\}$ and centre subspace $E^c = \{(x, y) : y = -x\}$. Hence, the stable manifold and centre manifold of this pitchfork bifurcation are given by

$$W^{\mathrm{s}} = \{(x, y) : y = x\},$$
$$W^{\mathrm{c}} = \left\{(x, y) : y = -x + \frac{1}{2\alpha}(x - \tilde{x}_2)^2 f''(\tilde{x}_2) - \frac{1}{4\alpha^2}(x - \tilde{x}_2)^3[f''(\tilde{x}_2)]^2 + O((x - \tilde{x}_2)^4)\right\}.$$

The bifurcation set is given by

$$\alpha\tilde{x}_2 = \sigma_1(\tilde{x}_2)\sigma_2(\tilde{x}_2),$$
$$\frac{1}{2}\beta_1(1 + \sigma_1)(1 - \sigma_1)\sigma_2 + \frac{\beta_2\sigma_1(\sigma_2 - 1)(k - \sigma_2)}{k - 1} = -\alpha. \tag{3.11}$$

In particular, we can compute the limit value of β_2 as $\beta_1 \to \infty$. Specifically, as $\beta_1 \to \infty$, $\sigma_1 \to 1$, $\sigma_1' \to 0$ and $\tilde{x}_2 \to \sigma_2/\alpha > 0$. Therefore, the limit value $\bar{\beta}_2$ must satisfy

$$\frac{\bar{\beta}_2(\sigma_2 - 1)(k - \sigma_2)}{k - 1} = -\alpha, \qquad \sigma_2 = \frac{1 + k\exp[\bar{\beta}_2(\sigma_2/\alpha - h)]}{1 + \exp[\bar{\beta}_2(\sigma_2/\alpha - h)]}. \tag{3.12}$$

When $\alpha = 1$, $k = -0.8$, $h = 0.5$, we obtain $\bar{\beta}_2 = 2.341\,96$. The surface in the parameter space described by (3.11) is the boundary between the regions where (2.3) has three or seven equilibria.

Seven equilibria. When $\mu_2 = f'(\tilde{x}_2) < -\alpha$, equilibrium E_2 becomes a saddle (see figure 2(*b*)) since two eigenvalues of the characteristic equation have opposite signs. In addition to three equilibria E_1, E_2, E_3 and two heteroclinic orbits E_1E_2 and E_1E_3, there appear four new intersections of the curves $y = f(x)/\alpha$ and $x = f(y)/\alpha$: $E_4(\tilde{x}_4, \tilde{y}_4)$, $E_5(\tilde{y}_4, \tilde{x}_4)$, $E_6(-\tilde{x}_4, -\tilde{y}_4)$, $E_7(-\tilde{y}_4, -\tilde{x}_4)$ with $\tilde{y}_4 > \tilde{x}_4 > 0$.

Let $\mu_3 = f'(\tilde{x}_4)$, $\mu_4 = f'(\tilde{y}_4)$ with $\tilde{y}_4 > \tilde{x}_4 > 0$. It is clear that $\mu_3 > -\alpha$, $\mu_4 < -\alpha$ and $\mu_3\mu_4 < \alpha^2$. Equilibrium E_4 is a stable node when $0 \leqslant \mu_3\mu_4 < \alpha^2$ and a stable focus when $\mu_3\mu_4 < 0$. Figure 2(*b*) shows the phase portrait where (2.3) has seven equilibria: three saddles E_1, E_2, E_3 and four stable foci E_4, E_5, E_6, E_7.

If two curves $y = f(x)/\alpha$ and $x = f(x)/\alpha$ intersect in the second and fourth quadrants and are tangent to each other, we see the appearance of two new steady states symmetric with respect to the origin and two new heteroclinic orbits: $E_8(\tilde{x}_8, \tilde{y}_8)$ and $E_9(-\tilde{x}_8, -\tilde{y}_8)$ with $x_8 > 0$ and $y_8 = -x_8$, and E_1E_8, E_1E_9 (heteroclinic orbits). Let $\mu_5 = f'(\tilde{x}_8)$. In such a case, $\mu_5 = -\alpha$. Since one eigenvalue of the characteristic equation at E_8 is zero, a saddle-node bifurcation occurs. The stable manifold and centre manifold of this saddle-node bifurcation are given by

$$W^{\mathrm{c}} = \{(x, y) : y = -x\},$$

$$W^{\mathrm{s}} = \left\{(x, y) : y = x - \frac{1}{4\alpha}(x - \tilde{x}_8)^2 f''(\tilde{x}_8) + \frac{1}{16\alpha^2}(x - \tilde{x}_8)^3[f''(\tilde{x}_8)]^2 + O((x - \tilde{x}_8)^4)\right\}.$$

This saddle-node bifurcation increases the number of stable equilibria to six. The bifurcation set is given by

$$\begin{aligned} &-\alpha\tilde{x}_8 = \sigma_1(\tilde{x}_8)\sigma_2(\tilde{x}_8), \\ &\frac{1}{2}\beta_1(1 + \sigma_1)(1 - \sigma_1)\sigma_2 + \frac{\beta_2\sigma_1(\sigma_2 - 1)(k - \sigma_2)}{k - 1} = -\alpha. \end{aligned} \tag{3.13}$$

In particular, we can compute the limit value of β_2 as $\beta_1 \to \infty$. Specifically, as $\beta_1 \to \infty$, $\sigma_1 \to 1$, $\sigma_1' \to 0$, $\tilde{x}_8 \to -\sigma_2/\alpha$ and $\sigma_2 < 0$. Therefore, the limit value $\bar{\beta}_2$ must satisfy

$$\frac{\bar{\beta}_2(\sigma_2 - 1)(k - \sigma_2)}{k - 1} = -\alpha, \qquad \sigma_2 = \frac{1 + k\exp[\bar{\beta}_2(-\sigma_2/\alpha - h)]}{1 + \exp[\bar{\beta}_2(-\sigma_2/\alpha - h)]}.$$

When $\alpha = 1$, $k = -0.8$, $h = 0.5$, we obtain $\bar{\beta}_2 = 13.9355$. The surface in the parameter space described by (3.13) is the boundary between the regions where (2.3) has seven equilibria or eleven equilibria. Figure 3(*a*) shows the phase portrait in this case where (2.3) undergoes saddle-node bifurcations at E_8 and E_9.

Eleven equilibria. As $\mu_5 < -\alpha$, the two curves $y = f(x)/\alpha$ and $x = f(y)/\alpha$ have now two intersections $E_{10}(\tilde{x}_{10}, \tilde{y}_{10})$ and $E_{11}(-\tilde{x}_{10}, -\tilde{y}_{10})$ with $\tilde{x}_{10} > 0$ and $\tilde{y}_{10} = -\tilde{x}_{10}$ in each of the second and fourth quadrants, as well as two new heteroclinic orbits E_8E_{10} and E_9E_{11}, as shown in figure 3(*b*). By theorem 3.1 with $\mu = \tilde{\mu} = \mu_5$, equilibrium E_8 becomes a saddle since two eigenvalues of the characteristic equation have opposite signs.

Let $\mu_6 = f'(\tilde{x}_{10})$ be the slope of the curve $y = f(x)$ at $E_{10}(\tilde{x}_{10}, \tilde{y}_{10})$. It is clear that $-\alpha < \mu_6 < 0$. By theorem 3.1 with $\mu = \tilde{\mu} = \mu_6$, equilibrium E_{10} is asymptotically stable. Figure 3(*b*) shows the phase portrait in this case where (2.3) has five saddles E_1, E_2, E_3, E_8, E_9, four stable foci E_4, E_5, E_6, E_7 and two stable nodes E_{10}, E_{11}.

In summary, one equilibrium, three equilibria with two heteroclinic orbits, seven equilibria with two heteroclinic orbits or eleven equilibria with six heteroclinic orbits can coexist in system (2.3), depending on values of the parameters α, β_1, β_2, k, h. Figure 4 shows the bifurcation sets of (2.3) in the (β_1, β_2)-plane and different regions where (2.3) has one, three,

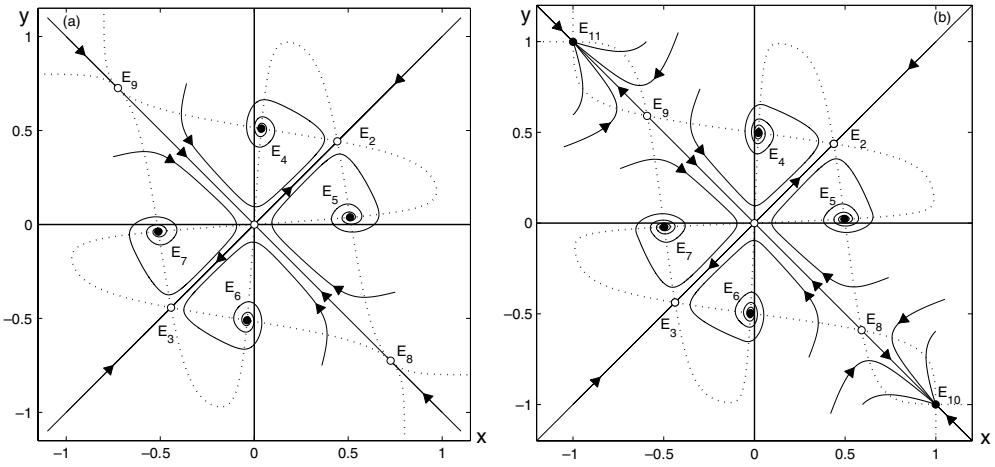

Figure 3. Phase portrait of (2.3) with saddle-node bifurcations (a) and eleven equilibria (b), where the dotted curves are graphs of $y = f(x)/\alpha$ and $x = f(y)/\alpha$.

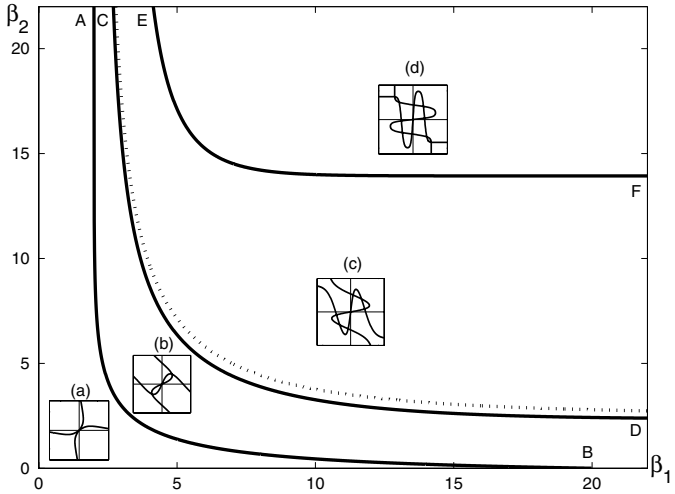

Figure 4. The bifurcation sets of (2.3) in the (β_1, β_2)-plane and different regions where (2.3) has one, three, seven and eleven equilibria when $\tau = 0$, $\alpha = 1$, $k = -0.8$ and $h = 0.5$. Curves AB, CD and EF represent bifurcation sets corresponding to equations (3.8), (3.11), (3.13), respectively. The dotted curve between CD and EF is where $\mu_3\mu_4 = 0$, which separates the region (c) into two areas. In the area between CD and the dotted curve, E_4, E_5, E_6, E_7 are stable nodes, and in the area between the dotted curve and EF these equilibria are stable foci. There is one stable equilibrium in the region (a); three equilibria in the region (b); seven equilibria in the region (c); eleven equilibria in the region (d).

seven and eleven equilibria when $\tau = 0$, $\alpha = 1$, $k = -0.8$ and $h = 0.5$. Curves AB, CD and EF represent bifurcation sets corresponding to equations (3.8), (3.11), (3.13), and they are boundaries between the regions with different numbers of equilibria in the parameter space. The limit value of β_2 is 2.341 96 for the curve CD, and 13.9355 for the curve EF as $\beta_1 \to \infty$. The dotted curve between CD and EF corresponds to $\mu_3\mu_4 = 0$, which separates the region (c) into two areas. In the area between CD and the dotted curve, E_4, E_5, E_6, E_7 are stable nodes, and in the area between the dotted curve and EF these equilibria are stable foci.

Table 1. Stability of equilibria of system (2.3) in different regions of Figure 4.

Equilibria	Region (a)	Curve AB	Region (b)	Curve CD	Region (c)	Curve EF	Region (d)
E_1	Stable	Pitchfork	Unstable	Unstable	Unstable	Unstable	Unstable
E_2, E_3	—	—	Stable	Pitchfork	Unstable	Unstable	Unstable
E_4, E_5, E_6, E_7	—	—	—	—	Stable	Stable	Stable
E_8, E_9	—	—	—	—	—	Saddlenode	Unstable
E_{10}, E_{11}	—	—	—	—	—	—	Stable
No of equilibria	1	1	3	3	7	9	11

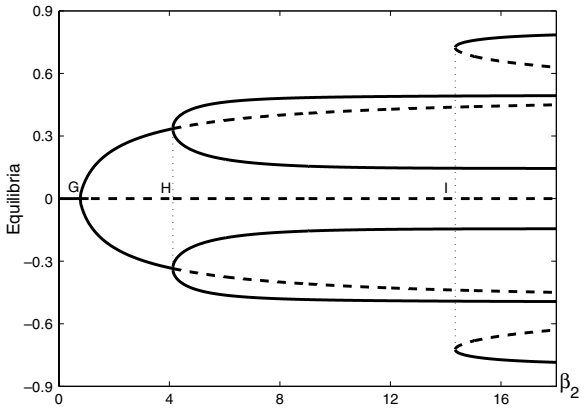

Figure 5. The bifurcation diagram in the $(\tilde{x}, \beta_2)$-plane when $\alpha = 1$, $\beta_1 = 7.5$, $k = -0.8$ and $h = 0.5$. Solid curves correspond to stable equilibria; dashed curves correspond to unstable equilibria (saddles). Bifurcation values are $\beta_2 = 0.749\,387$ (G), $\beta_2 = 4.124\,125$ (H) and $\beta_2 = 14.343\,59$ (I).

There is one stable equilibrium $E_1(0, 0)$ in the region (a); three equilibria in the region (b): one saddle E_1, two stable nodes E_2, E_3; seven equilibria in the region (c): three saddles E_1, E_2, E_3, four stable nodes or four stable foci; and eleven equilibria in the region (d): five saddles, four stable foci and two stable nodes E_{10}, E_{11}. Table 1 lists the stability of equilibria of system (2.3) in different regions of figure 4.

Figure 5 shows the bifurcation diagram in the $(\tilde{x}, \beta_2)$-plane when $\tau = 0, \alpha = 1, \beta_1 = 7.5$, $k = -0.8$ and $h = 0.5$. There exist three bifurcations: a supercritical pitchfork bifurcation at $\beta_2 = 0.749\,387$ (labelled as G in the Figure), a supercritical pitchfork bifurcation at $\beta_2 = 4.124\,125$ (labelled as H) and a saddle-node bifurcation at $\beta_2 = 14.343\,59$ (labelled as I).

Multistability in the form of the coexistence of multiple stable equilibria occurs when $\beta_2 > 0.749\,387$, as shown in figure 5: when $0.749\,387 < \beta_2 < 4.124\,125$, there are two stable equilibria; when $4.124\,125 < \beta_2 < 14.343\,59$, there are four stable equilibria; when $\beta_2 > 14.343\,59$, there are six stable equilibria.

4. Effect of τ on stability and multistability

We now address the impact of time lag τ on the stability of the equilibria. When $\tau > 0$, the linearized system of (2.3) at an equilibrium, $(\tilde{x}, \tilde{y})$, is given by

$$x_1'(t) = -\alpha x_1 + f'(\tilde{y})x_2(t-\tau) = -\alpha x_1 + \tilde{\mu}x_2(t-\tau),$$
$$x_2'(t) = -\alpha x_2 + f'(\tilde{x})x_1(t-\tau) = -\alpha x_2 + \mu x_1(t-\tau),$$

where $(x_1(t), x_2(t)) = (x(t) - \tilde{x}, y(t) - \tilde{y})$, $\mu = f'(\tilde{x})$ and $\tilde{\mu} = f'(\tilde{y})$. The characteristic equation is given by

$$\det \begin{pmatrix} \lambda + \alpha & -\tilde{\mu} e^{-\lambda\tau} \\ -\mu e^{-\lambda\tau} & \lambda + \alpha \end{pmatrix} = 0.$$

That is,

$$(\lambda + \alpha)^2 - \mu\tilde{\mu} e^{-2\lambda\tau} = 0. \tag{4.14}$$

Since $\mu = \tilde{\mu}$ if and only if the equilibrium is on the line $y = x$ or $y = -x$, we shall distinguish two cases: for those on the lines $y = x$ and $y = -x$, and for those off the lines.

Stability of equilibria on the lines $y = x$ and $y = -x$. Obviously, equilibria on the lines $y = x$ and $y = -x$ are $E_1, E_2, E_3, E_8, E_9, E_{10}, E_{11}$. Let $\lambda = \gamma + i\omega$, $\gamma, \omega \in \mathbb{R}$. Equation (4.14) with $\mu = \tilde{\mu}$ gives rise to

$$(\gamma + \alpha)^2 - \omega^2 = \mu^2 e^{-2\gamma\tau} \cos(2\omega\tau), \qquad 2\omega(\gamma + \alpha) = -\mu^2 e^{-2\gamma\tau} \sin(2\omega\tau). \tag{4.15}$$

Squaring and adding two equations of (4.15), we obtain

$$(\gamma + \alpha)^2 + \omega^2 = \mu^2 e^{-2\gamma\tau}. \tag{4.16}$$

Adding the first equation in (4.15) to equation (4.16) yields

$$\gamma = -\alpha \pm |\mu| e^{-\gamma\tau} \cos(\omega\tau). \tag{4.17}$$

It is straightforward to verify that

Theorem 4.1. *If parameters satisfy $|\mu| < \alpha$, all eigenvalues λ of equation (4.14) have negative real parts.*

As an immediate consequence, we obtain

Lemma 4.2. *Stable equilibria on the lines $y = x$ and $y = -x$ with the instantaneous feedback remain to be stable when $\tau > 0$.*

Hence, equilibrium E_1 in the region (a) of figure 4, equilibria E_2 and E_3 in the region (b) of figure 4, equilibria E_{10} and E_{11} in the region (d) of figure 4 are all stable when $\tau > 0$.

Theorem 4.3. *If parameters satisfy $|\mu| = \alpha$, equation (4.14) always has one eigenvalue $\lambda = 0$ for all $\tau \geqslant 0$, and all other eigenvalues have negative real parts.*

Proof. It is easy to check that $\lambda = 0$ is one solution of equation (4.14) for all $\tau \geqslant 0$. Under the condition of the theorem, equation (4.17) becomes

$$\frac{\gamma}{\alpha} = -1 \pm e^{-\gamma\tau} \cos(\omega\tau). \tag{4.18}$$

Suppose $\gamma > 0$. Then

$$\frac{\gamma}{\alpha} = -1 \pm e^{-\gamma\tau} \cos(\omega\tau) \leqslant -1 + e^{-\gamma\tau} \leqslant 0,$$

a contradiction to our assumption. Hence, $\gamma \leqslant 0$. Equation (4.16) leads to $(\gamma + \alpha)^2 + \omega^2 = \alpha^2 e^{-2\gamma\tau}$. When $\gamma = 0$, it yields $\omega = 0$, i.e. $\lambda = 0$. Hence for $\lambda \neq 0$, the real part γ must satisfy $\gamma < 0$. □

Lemma 4.4. *Steady-state bifurcations occurring in the instantaneous feedback case also take place when $\tau > 0$.*

Thus, the supercritical pitchfork bifurcations on the curve AB, CD and the saddle-node bifurcation on the curve EF of figure 4 also take place when $\tau > 0$.

The following two theorems suggest that Hopf bifurcations can occur when $|\mu| > \alpha$, creating unstable periodic solutions:

Theorem 4.5. *If parameters satisfy $|\mu| > \alpha$, the characteristic equation (4.14) has a pair of purely imaginary eigenvalues $\lambda = \pm i\omega$ satisfying*

$$\omega = \sqrt{\mu^2 - \alpha^2}, \tag{4.19}$$

when τ takes the following values

$$\tau_j = \frac{1}{2\sqrt{\mu^2-\alpha^2}} \begin{cases} \left[\arctan\left(\dfrac{2\alpha\sqrt{\mu^2-\alpha^2}}{\mu^2-2\alpha^2}\right) + 2j\pi\right] & \text{if } \alpha < |\mu| \leqslant \sqrt{2}\alpha, \\ \left[\arctan\left(\dfrac{2\alpha\sqrt{\mu^2-\alpha^2}}{\mu^2-2\alpha^2}\right) + (2j+1)\pi\right] & \text{if } |\mu| > \sqrt{2}\alpha \end{cases} \tag{4.20}$$

for $j = 0, 1, 2, \ldots$, where arctan *is the principal branch of the inverse tangent function.*

Proof. Let $\lambda = i\omega$ with $\omega > 0$. Equation (4.16) yields

$$\omega = \sqrt{\mu^2 - \alpha^2}.$$

It easily follows from system (4.15) that $\sin(2\omega\tau)$ is always negative and the sign of $\cos(2\omega\tau)$ depends on the value of $\mu^2 - 2\alpha^2$. Dividing the second equation by the first equation of (4.15) leads to equation (4.20). It is clear that ω is well-defined if and only if $|\mu| > \alpha$. □

Theorem 4.6. *If parameters satisfy $|\mu| > \alpha$, equation (4.14) always has a positive eigenvalue.*

Proof. We consider the real eigenvalue of equation (4.14). Equation (4.14) yields $\lambda = -\alpha \pm |\mu|e^{-\lambda\tau}$ where λ is the real value. Let $g(\lambda) = \lambda + \alpha - |\mu|e^{-\lambda\tau}$. It is clear that $g(0) = \alpha - |\mu| < 0$ under the condition of $|\mu| > \alpha$. Furthermore, $\lim_{\lambda\to\infty} g(\lambda) = +\infty$. Hence, there exists $\lambda_0 > 0$ satisfying $g(\lambda_0) = 0$. □

Lemma 4.7. *An equilibrium on the line $y = x$ or line $y = -x$ remains unstable for $\tau > 0$ if it is unstable in the instantaneous feedback case.*

Stability of equilibria E_4, E_5, E_6, E_7. Let $(\tilde{x}, \tilde{y})$ be one of equilibria $E_4, E_5, E_6\ E_7$ and $\mu = f'(\tilde{x})$, $\tilde{\mu} = f'(\tilde{y})$. It follows from the bifurcation process discussed in section 3 that $\mu\tilde{\mu} < \alpha^2$. Let $\lambda = \gamma + i\omega$, $\gamma, \omega \in \mathbb{R}$. For the equilibria E_4, E_5, E_6, E_7, equation (4.14) gives rise to

$$(\gamma+\alpha)^2 - \omega^2 = \mu\tilde{\mu}e^{-2\gamma\tau}\cos(2\omega\tau), \qquad 2\omega(\gamma+\alpha) = -\mu\tilde{\mu}e^{-2\gamma\tau}\sin(2\omega\tau). \tag{4.21}$$

Squaring and adding two equations of (4.21), we obtain

$$(\gamma+\alpha)^2 + \omega^2 = |\mu\tilde{\mu}|e^{-2\gamma\tau}. \tag{4.22}$$

Adding the first equation in (4.21) to equation (4.22) yields

$$\gamma = \begin{cases} -\alpha \pm \sqrt{|\mu\tilde{\mu}|}e^{-\gamma\tau}\cos(\omega\tau) & \text{if } \mu\tilde{\mu} \geqslant 0; \\ -\alpha \pm \sqrt{|\mu\tilde{\mu}|}e^{-\gamma\tau}\sin(\omega\tau) & \text{if } \mu\tilde{\mu} < 0. \end{cases} \tag{4.23}$$

In case where $0 \leqslant \mu\tilde{\mu} < \alpha^2$, applying theorem 4.1 with μ replaced by $\sqrt{\mu\tilde{\mu}}$, we obtain the following

Lemma 4.8. *If parameters satisfy $0 \leqslant \mu\tilde{\mu} < \alpha^2$, equilibria E_4, E_5, E_6, E_7 preserve their stability when $\tau > 0$.*

Theorem 4.9. *If parameters satisfy $-\alpha^2 \leqslant \mu\tilde{\mu} < 0$, all eigenvalues λ of equation (4.14) have negative real parts.*

Proof. Under the condition $-\alpha^2 \leqslant \mu\tilde{\mu} < 0$, it easily follows from equation (4.14) that $\lambda \neq 0$. We first prove that the real part γ of λ must be negative when $-\alpha^2 < \mu\tilde{\mu} < 0$. Suppose that $\gamma > 0$. Equation (4.23) becomes

$$\gamma = -\alpha \pm \sqrt{|\mu\tilde{\mu}|}\mathrm{e}^{-\gamma\tau}\sin(\omega\tau) \leqslant -\alpha + \sqrt{|\mu\tilde{\mu}|}\mathrm{e}^{-\gamma\tau} \leqslant -\alpha + \sqrt{|\mu\tilde{\mu}|} < 0, \tag{4.24}$$

a contradiction to our assumption. Then suppose $\gamma = 0$. Equation (4.22) yields $\alpha^2 + \omega^2 = |\mu\tilde{\mu}|$, a contradiction to the condition $-\alpha^2 < \mu\tilde{\mu} < 0$. Hence, γ must be negative for $-\alpha^2 < \mu\tilde{\mu} < 0$.

Now we consider $\mu\tilde{\mu} = -\alpha^2$. Equation (4.22) leads to $(\gamma + \alpha)^2 + \omega^2 = \alpha^2\mathrm{e}^{-2\gamma\tau}$. It follows from $\lambda \neq 0$ that $\gamma \neq 0$. Suppose $\gamma > 0$. The above equation (4.24) yields $\gamma \leqslant 0$, a contradiction to our assumption. Thus γ must be negative for $\mu\tilde{\mu} = -\alpha^2$. This completes our proof. □

Lemma 4.10. *If parameters satisfy $-\alpha^2 \leqslant \mu\tilde{\mu} < \alpha^2$, equilibria E_4, E_5, E_6, E_7 preserve their stability when $\tau > 0$.*

Theorem 4.11. *For $\mu\tilde{\mu} < -\alpha^2$, we have the following:*

(i) Equation (4.14) has a pair of purely imaginary eigenvalues $\lambda = \pm\mathrm{i}\omega$ satisfying

$$\omega = \sqrt{|\mu\tilde{\mu}| - \alpha^2}, \tag{4.25}$$

when τ takes the following values

$$\tau_j = \frac{1}{2\sqrt{|\mu\tilde{\mu}| - \alpha^2}} \times \begin{cases} \left[\arctan\left(\dfrac{2\alpha\sqrt{|\mu\tilde{\mu}| - \alpha^2}}{|\mu\tilde{\mu}| - 2\alpha^2}\right) + (2j+1)\pi\right] & \text{if } -2\alpha^2 \leqslant \mu\tilde{\mu} < -\alpha^2, \\ \left[\arctan\left(\dfrac{2\alpha\sqrt{|\mu\tilde{\mu}| - \alpha^2}}{|\mu\tilde{\mu}| - 2\alpha^2}\right) + 2j\pi\right] & \text{if } \mu\tilde{\mu} < -2\alpha^2 \end{cases} \tag{4.26}$$

for $j = 0, 1, 2, \ldots$, where arctan *is the principal branch of the inverse tangent function;*

(ii) For $\tau \in [0, \tau_0)$, all eigenvalues of the characteristic equation (4.14) have negative real parts;

(iii) When $\tau = \tau_0$, except $\lambda = \pm\mathrm{i}\omega$, all other eigenvalues of equation (4.14) have negative real parts;

(iv) When $\tau \in (\tau_{j-1}, \tau_j)$ with $j = 1, 2, \ldots$, equation (4.14) has $2j$ eigenvalues with positive real parts.

Proof. Equation (4.22) with $\lambda = i\omega$ immediately leads to (4.25). Since $\mu\tilde{\mu} < 0$, it easily follows from system (4.21) that $\sin(2\omega\tau)$ is always positive and the sign of $\cos(2\omega\tau)$ depends on the value of $|\mu\tilde{\mu}| - 2\alpha^2$. Dividing the second equation by the first equation of (4.21) yields (4.26).

Let $\lambda(\tau) = \gamma(\tau) + \mathrm{i}\omega(\tau)$ be a solution of (4.14). Since the roots of (4.14) continuously depend on the parameter τ, $\gamma(\tau)$ is a continuous function with respect to τ. It follows from equation (4.23) with $\mu\tilde{\mu} < 0$ that $\gamma(0) = -\alpha$ is always negative. Furthermore, τ_0 is the first time that a pair of conjugate complex eigenvalues crosses the imaginary axis in the complex plane. This implies that $\gamma(\tau) < 0$ on the interval $\tau \in [0, \tau_0)$ for all eigenvalues λ. Hence, (ii) and (iii) hold.

Differentiating equation (4.14) with respect to τ gives rise to

$$\frac{\mathrm{d}\lambda}{\mathrm{d}\tau} = \frac{-\mu\tilde{\mu}\lambda \mathrm{e}^{-2\lambda\tau}}{\lambda + \alpha + \mu\tilde{\mu}\tau \mathrm{e}^{-2\lambda\tau}} = \frac{-\lambda(\lambda+\alpha)}{1+\tau(\lambda+\alpha)}$$
$$= -\frac{(\gamma + \mathrm{i}\omega)(\gamma + \alpha + \mathrm{i}\omega)(1 + \tau\alpha + \tau\gamma - \mathrm{i}\tau\omega)}{(1 + \tau\alpha + \tau\gamma)^2 + (\tau\omega)^2}.$$

It follows

$$\frac{\mathrm{d}\,\mathrm{Re}\,\lambda}{\mathrm{d}\tau} = -\frac{(\gamma^2 + \gamma\alpha - \omega^2)(1 + \tau\alpha + \tau\gamma) + \tau\omega^2(2\gamma + \alpha)}{(1 + \tau\alpha + \tau\gamma)^2 + (\tau\omega)^2}.$$

At $\lambda = \pm\mathrm{i}\omega$, we have

$$\left.\frac{\mathrm{d}\,\mathrm{Re}\,\lambda}{\mathrm{d}\tau}\right|_{\lambda=\pm\mathrm{i}\omega} = \frac{\omega^2}{(1+\tau\alpha)^2 + (\tau\omega)^2} > 0.$$

A pair of conjugate complex eigenvalues always crosses the imaginary axis from the left half plane to the right half plane in the complex plane when $\tau = \tau_j$ for $j = 0, 1, 2, \ldots$. Thus, the number of eigenvalues with positive real parts increases by 2. This gives the result of (iv). □

Lemma 4.12. *If parameters satisfy $\mu\tilde{\mu} < -\alpha^2$, the four equilibria E_4, E_5, E_6, E_7 have the following properties:*

(i) they are asymptotically stable when $\tau \in [0, \tau_0)$;
(ii) they are all unstable when $\tau > \tau_0$;
(iii) there is a pair of purely imaginary eigenvalues $\lambda = \pm\mathrm{i}\omega$ at $\tau = \tau_j$ with $j = 0, 1, 2, \ldots$, for the linearization at these equilibria.

We now summarize our results in figures 6 and 7. Figure 6 shows the areas (labelled by (c_3), (d) and filled by colour) in the (β_1, β_2)-plane where increasing the delay may affect the stability of equilibria E_4, E_5, E_6, E_7. Note that the curves JK and PQ are the segments of CD and EF in figure 4, respectively. Two curves NO (thin solid curve, $\mu\tilde{\mu} = -\alpha^2$) and LM (dotted curve, $\mu\tilde{\mu} = 0$) separate the region (c) of figure 4 into three parts: (c_1), (c_2) and (c_3). In areas (c_1) and (c_2) including the two curves NO and LM, increasing τ does not change the stability of the four equilibria, i.e. they remain stable. In areas (c_3) and (d) where $\mu\tilde{\mu} < -\alpha^2$, the four equilibria are asymptotically stable when $\tau \in [0, \tau_0)$; when $\tau = \tau_0$, the four equilibria lose their stability, a pair of purely imaginary eigenvalues $\lambda = \pm\mathrm{i}\omega$ appears and a Hopf bifurcation may occur; when $\tau > \tau_0$, the four equilibria become unstable and periodic limit cycles appear, as will be shown in section 5.

Figure 7 shows the stability diagram in the (μ_0, τ)-plane with $\mu_0 = \mu\tilde{\mu}$ when $\alpha = 1$. In the filled area corresponding to either $|\mu\tilde{\mu}| \leqslant \alpha^2$ or $\mu\tilde{\mu} < -\alpha^2$ but $\tau < \tau_0$, local asymptotic stability of equilibria E_4, E_5, E_6, E_7 holds. On the other hand, if $\mu\tilde{\mu} < -\alpha^2$ and $\tau > \tau_0$, these equilibria lose their stability and become unstable.

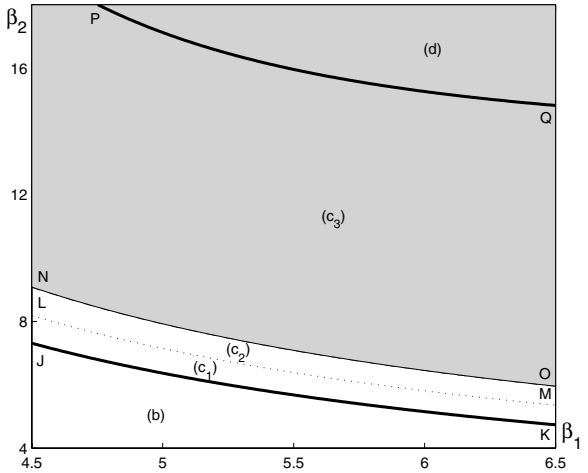

Figure 6. Increasing τ beyond τ_0 only affects the stability of equilibria E_4, E_5, E_6, E_7 in filled areas (c_3) and (d) in the (β_1, β_2)-plane of figure 4. Note that the curves JK and PQ are the segments of CD and EF in figure 4, respectively. Two curves NO (thin solid curve, $\mu\tilde{\mu} = -\alpha^2$) and LM (dotted curve, $\mu\tilde{\mu} = 0$) separate the region (c) of figure 4 into three parts: (c_1), (c_2) and (c_3). In areas (c_1) and (c_2) including curves NO and LM, increasing τ does not change the stability of these four equilibria, i.e. they remain stable.

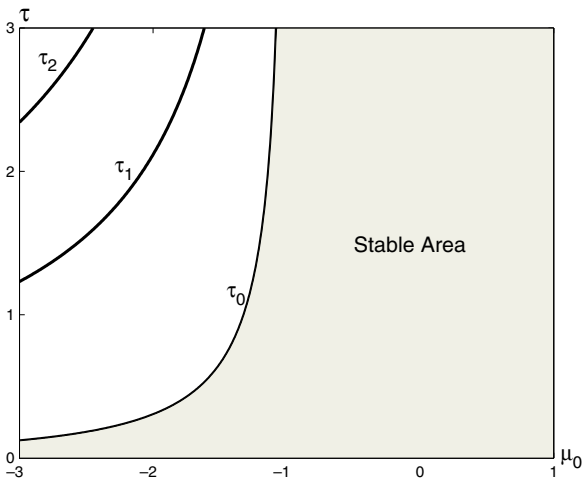

Figure 7. Stability diagram in the (μ_0, τ)-plane with $\mu_0 = \mu\tilde{\mu}$ when $\alpha = 1$. Local asymptotic stability of equilibria E_4, E_5, E_6, E_7 holds in the filled area.

5. Hopf bifurcation

In the previous section, we studied the effect of τ on the stability of equilibria obtained in section 3. We found that if $\mu\tilde{\mu} < -\alpha^2$, as τ increases to τ_0, a pair of complex conjugate eigenvalues associated with equilibria E_4, E_5, E_6, E_7 passes through the imaginary axis, indicating the possibility of a Hopf bifurcation.

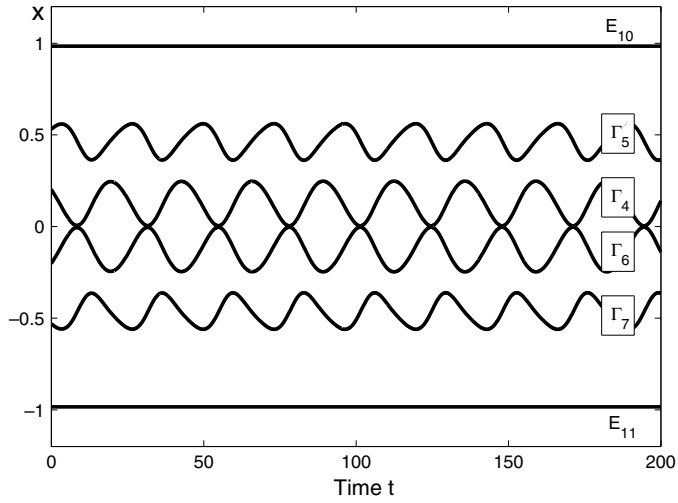

Figure 8. Four stable limit cycles $\Gamma_4, \Gamma_5, \Gamma_6, \Gamma_7$ bifurcated from equilibria E_4, E_5, E_6, E_7 coexist with two stable equilibria E_{10}, E_{11} when $\tau > \tau_0$. In this figure, $\alpha = 1$, $\beta_1 = \beta_2 = 10$, $k = -1$, $h = 0.5$ and $\tau = 0.079$, and these parameters locate at the region (d) of figure 4 where there exist eleven equilibria.

It is clear that $\lambda = \mathrm{i}\omega$ with $\omega = \sqrt{|\mu\tilde{\mu}| - \alpha^2}$ is a simple eigenvalue. Furthermore, in the proof of theorem 4.11, we have obtained the transversality condition

$$\left.\frac{\mathrm{d}\,\mathrm{Re}\,\lambda}{\mathrm{d}\tau}\right|_{\lambda=\pm\mathrm{i}\omega} = \frac{\omega^2}{(1+\tau\alpha)^2 + (\tau\omega)^2} > 0.$$

Therefore, when $\tau = \tau_j$ for $j = 0, 1, 2, \ldots$, system (2.3) undergoes Hopf bifurcations at equilibria E_4, E_5, E_6, E_7 simultaneously, which result in the change of stability of these equilibria. When $\tau > \tau_0$, one periodic limit cycle around each equilibrium appears. We observe six coexisting stable patterns shown in figure 8: two stable nodes E_{10}, E_{11}, four stable periodic limit cycles Γ_4, Γ_5, Γ_6, Γ_7 which surround equilibria E_4, E_5, E_6, E_7, respectively.

In the remaining part of this section, we use the centre manifold reduction and the normal form calculation developed in [3, 23] to study the direction of the Hopf bifurcation, stability and period of the bifurcated periodic solutions around the equilibrium E_4, whose coordinate is denoted by $(\tilde{x}, \tilde{y})$ in this section. Delay τ is restricted to a small neighbourhood of τ_0. Let $(x_1(t), x_2(t)) = (x(\tau t) - \tilde{x}, y(\tau t) - \tilde{y})$. Expanding function f at the equilibrium $E_4(\tilde{x}, \tilde{y})$, we obtain the following differential equations:

$$x_1'(t) = -\alpha\tau x_1(t) + \tau\tilde{\mu}x_2(t-1) + \tau\frac{f''(\tilde{y})}{2}x_2^2(t-1) + \tau\frac{f'''(\tilde{y})}{6}x_2^3(t-1) + O(x_2^4), \tag{5.27}$$

$$x_2'(t) = -\alpha\tau x_2(t) + \tau\mu x_1(t-1) + \tau\frac{f''(\tilde{x})}{2}x_1^2(t-1) + \tau\frac{f'''(\tilde{x})}{6}x_1^3(t-1) + O(x_1^4), \tag{5.28}$$

with $\mu = f'(\tilde{x})$ and $\tilde{\mu} = f'(\tilde{y})$. Equations (5.27) and (5.28) can also be expressed in the general setting as follows:

$$\begin{aligned} &X'(t) = A_1X(t) + A_2X_t(-1) + F(X_t(-1)),\\ &A_1 = \begin{pmatrix} -\alpha\tau & 0 \\ 0 & -\alpha\tau \end{pmatrix}, \qquad A_2 = \begin{pmatrix} 0 & \tau\tilde{\mu} \\ \tau\mu & 0 \end{pmatrix} \end{aligned} \tag{5.29}$$

with $X(t) = (x_1(t), x_2(t))^T$, $X_t(s) \in C_2 := C \times C$, where $C = C([-1, 0]; \mathbb{R})$, is defined by $X_t(s) = X(t + s)$ for $s \in [-1, 0]$, and

$$F(X_t(-1)) := \begin{pmatrix} F_1(x_{2,t}(-1)) \\ F_2(x_{1,t}(-1)) \end{pmatrix} = \begin{pmatrix} b_2 x_{2,t}^2(-1) + b_3 x_{2,t}^3(-1) \\ a_2 x_{1,t}^2(-1) + a_3 x_{1,t}^3(-1) \end{pmatrix} + O(||X_t||^4), \tag{5.30}$$

where

$$a_2 = \tau \frac{f''(\tilde{x})}{2}, \quad a_3 = \tau \frac{f'''(\tilde{x})}{6}, \quad b_2 = \tau \frac{f''(\tilde{y})}{2}, \quad b_3 = \tau \frac{f'''(\tilde{y})}{6}.$$

Let $L : C_2 \to \mathbb{R}^2$ be a linear operator given by $L\varphi = A_1\varphi(0) + A_2\varphi(-1)$. There exists a 2×2 matrix $\eta : [-1, 0] \to \mathbb{R}^{2\times 2}$, whose elements are of bounded variation such that

$$L\varphi = \int_{-1}^{0} [\mathrm{d}\eta(\vartheta)]\varphi(\vartheta).$$

In the case of discrete delays, the function $\eta(\vartheta)$ can be expressed in terms of a step function $H(\vartheta)$,

$$\eta(\vartheta) = A_1 H(\vartheta) + A_2 H(\vartheta + 1), \qquad H(\vartheta) = \begin{cases} 0 & \text{if } \vartheta \in [-1, 0), \\ 1 & \text{if } \vartheta = 0. \end{cases}$$

For $\phi \in C_2([-1, 0] : \mathbb{R}^2)$ and $\psi \in C_2^{\mathrm{T}}([0, 1] : (\mathbb{R}^2)^{\mathrm{T}})$, we define two infinitesimal generators, A in phase space C_2 and A^{T} in the adjoint space C_2^{T}, as

$$A\phi = \begin{cases} \dot{\phi}(\vartheta) & \text{if } \vartheta \in [-1, 0), \\ \displaystyle\int_{-1}^{0} \mathrm{d}\eta(\vartheta)\phi(\vartheta) & \text{if } \vartheta = 0. \end{cases}$$

$$A^T\psi = \begin{cases} -\dot{\psi}(s) & \text{if } s \in (0, 1], \\ \displaystyle\int_{-1}^{0} \psi(-s)\mathrm{d}\eta^{\mathrm{T}}(s) & \text{if } s = 0, \end{cases}$$

and a bilinear form

$$\langle \psi, \phi \rangle = \bar{\psi}(0)\phi(0) - \int_{-1}^{0}\int_{0}^{\vartheta} \bar{\psi}(\xi - \vartheta)[\mathrm{d}\eta(\vartheta)]\phi(\xi)\,\mathrm{d}\xi.$$

Let

$$R\varphi = \begin{cases} 0 & \text{if } \vartheta \in [-1, 0), \\ F(\varphi) & \text{if } \vartheta = 0. \end{cases}$$

Then system (5.29) is equivalent to

$$\dot{X}_t = AX_t + RX_t. \tag{5.31}$$

The two infinitesimal generators A and A^{T} have the same eigenvalues $\pm \mathrm{i}\omega\tau_0$. Eigenvector q of A corresponding to $\lambda = \mathrm{i}\omega\tau_0$ and eigenvector p of A^{T} corresponding to $\lambda = -\mathrm{i}\omega\tau_0$ are given by

$$q(\vartheta) = \mathrm{e}^{\mathrm{i}\omega\tau_0\vartheta}(1, \bar{p}_0)^T, \qquad p(s) = D\mathrm{e}^{\mathrm{i}\omega\tau_0 s}(p_0, 1), \quad \text{where } p_0 = \frac{\mu \mathrm{e}^{\mathrm{i}\omega\tau_0}}{\alpha - \mathrm{i}\omega}$$

with $\vartheta \in [-1, 0]$ and $s \in [0, 1]$. In order that $< p, q >= 1$, we choose $D = \frac{1}{2p_0 + \tau_0(\mu + \tilde{\mu}p_0^2)\mathrm{e}^{\mathrm{i}\omega\tau_0}}$. Note that

$$\int_{-1}^{0} [\mathrm{d}\eta(\vartheta)]\mathrm{e}^{\mathrm{i}\omega\tau_0\vartheta} = \mathrm{i}\omega\tau_0 I_{2\times 2}, \qquad \int_{-1}^{0} [\mathrm{d}\eta(\vartheta)]\mathrm{e}^{-\mathrm{i}\omega\tau_0\vartheta} = -\mathrm{i}\omega\tau_0 I_{2\times 2}. \tag{5.32}$$

Using equations (5.32), it is easy to check that $< p, \bar{q} >= 0$.

We map real coordinate (x_1, x_2) into complex coordinate $\{(z, \bar{z}); z \in \mathbb{C}\}$ by $(x_1, x_2) \mapsto (x_1 + \mathrm{i}x_2, x_1 - \mathrm{i}x_2)$. Let $\Phi = (q, \bar{q})$ and $\Psi = (p, \bar{p})$. The centre manifold for the system (5.31) is given by

$$C_0 = \{zq + \bar{z}\bar{q} + W(z, \bar{z}, \vartheta)\},$$

where $z(t)$ satisfies the following ordinary differential equation

$$\dot{z}(t) = \mathrm{i}\omega\tau_0 z + \bar{p}(0)F(zq + \bar{z}\bar{q} + W(z, \bar{z}, \vartheta)) = \mathrm{i}\omega\tau_0 z + \bar{p}(0)F_0(z, \bar{z}) \quad (5.33)$$

with $F_0(z, \bar{z}) = F(zq+\bar{z}\bar{q}+W(z, \bar{z}, \vartheta))$. For the solution $X(t)$ of (5.31) on the centre manifold C_0, i.e. $X_t \in C_0$, $W(z, \bar{z}, \vartheta)$ satisfies

$$\dot{W} = \begin{cases} AW - \bar{p}(0)F_0(z, \bar{z})q(\vartheta) - p(0)\bar{F}_0(z, \bar{z})\bar{q}(\vartheta) & \text{if } \vartheta \in [-1, 0), \\ AW - \bar{p}(0)F_0(z, \bar{z})q(0) - p(0)\bar{F}_0(z, \bar{z})\bar{q}(0) + F_0(z, \bar{z}) & \text{if } \vartheta = 0. \end{cases} \quad (5.34)$$

We denote the above equation as $\dot{W} = AW + H(z, \bar{z}, \vartheta)$. On the centre manifold C_0 around $z = 0$, we have $\dot{W} = W_z\dot{z} + W_{\bar{z}}\dot{\bar{z}}$. Hence,

$$AW + H(z, \bar{z}, \vartheta) = W_z\dot{z} + W_{\bar{z}}\dot{\bar{z}}. \quad (5.35)$$

Our objective is to reformulate the explicit form of (5.33) in higher order terms of z and $\tilde{z}$. To achieve our goal, we need to know the Taylor series expansion of $F_0(z, \bar{z})$. Hence, we expand functions W, H in their Taylor series around $z = 0$,

$$W(z, \bar{z}, \vartheta) = W_{20}(\vartheta)\frac{z^2}{2} + W_{11}(\vartheta)z\bar{z} + W_{02}(\vartheta)\frac{\bar{z}^2}{2} + \cdots,$$

$$H(z, \bar{z}, \vartheta) = H_{20}(\vartheta)\frac{z^2}{2} + H_{11}(\vartheta)z\bar{z} + H_{02}(\vartheta)\frac{\bar{z}^2}{2} + \cdots.$$

Let $G(z, \bar{z}) = \bar{p}(0)F_0(z, \bar{z})$. It has the Taylor series expansion as

$$G(z, \bar{z}) = g_{20}\frac{z^2}{2} + g_{11}z\bar{z} + g_{02}\frac{\bar{z}^2}{2} + g_{21}\frac{z^2\bar{z}}{2}\cdots.$$

Noticing that $X_t(\vartheta) = (x_{1,t}(\vartheta), x_{2,t}(\vartheta))^{\mathrm{T}} = zq(\vartheta) + \bar{z}\bar{q}(\vartheta) + W(z, \bar{z}, \vartheta)$ and $q(\vartheta) = e^{i\omega\tau_0\vartheta}(1, \bar{p}_0)^{\mathrm{T}}$, we have

$$x_{1,t}(-1) = \mathrm{e}^{-\mathrm{i}\omega\tau_0}z + \mathrm{e}^{\mathrm{i}\omega\tau_0}\bar{z} + W_{20}^{(1)}(-1)\frac{z^2}{2} + W_{11}^{(1)}(-1)z\bar{z} + W_{02}^{(1)}(-1)\frac{\bar{z}^2}{2} + \cdots$$

$$x_{2,t}(-1) = \bar{p}_0\mathrm{e}^{-\mathrm{i}\omega\tau_0}z + p_0\mathrm{e}^{\mathrm{i}\omega\tau_0}\bar{z} + W_{20}^{(2)}(-1)\frac{z^2}{2} + W_{11}^{(2)}(-1)z\bar{z} + W_{02}^{(2)}(-1)\frac{\bar{z}^2}{2} + \cdots$$

Substituting $x_{1,t}(-1)$, $x_{2,t}(-1)$ into equation (5.30), we obtain

$$\begin{aligned} F_1(x_{2,t}(-1)) &= b_2\bar{p}_0^2\mathrm{e}^{-\mathrm{i}2\omega\tau_0}z^2 + 2b_2p_0\bar{p}_0z\bar{z} + b_2p_0^2\mathrm{e}^{\mathrm{i}2\omega\tau_0}\bar{z}^2 \\ &\quad + [2W_{11}^{(2)}(-1)b_2\bar{p}_0\mathrm{e}^{-\mathrm{i}\omega\tau_0} + W_{20}^{(2)}(-1)b_2p_0\mathrm{e}^{\mathrm{i}\omega\tau_0} + 3b_3p_0\bar{p}_0^2\mathrm{e}^{-\mathrm{i}\omega\tau_0}]z^2\bar{z} + \cdots \\ F_2(x_{1,t}(-1)) &= a_2\mathrm{e}^{-\mathrm{i}2\omega\tau_0}z^2 + 2a_2z\bar{z} + a_2\mathrm{e}^{\mathrm{i}2\omega\tau_0}\bar{z}^2 \\ &\quad + [2W_{11}^{(1)}(-1)a_2\mathrm{e}^{-\mathrm{i}\omega\tau_0} + W_{20}^{(1)}(-1)a_2\mathrm{e}^{\mathrm{i}\omega\tau_0} + 3a_3e^{-i\omega\tau_0}]z^2\bar{z} + \cdots. \end{aligned}$$

Hence,

$$F_0(z, \bar{z}) = \begin{pmatrix} b_2\bar{p}_0^2\mathrm{e}^{-\mathrm{i}2\omega\tau_0} \\ a_2\mathrm{e}^{-\mathrm{i}2\omega\tau_0} \end{pmatrix} z^2 + \begin{pmatrix} 2b_2p_0\bar{p}_0 \\ 2a_2 \end{pmatrix} z\bar{z} + \begin{pmatrix} b_2p_0^2\mathrm{e}^{\mathrm{i}2\omega\tau_0} \\ a_2\mathrm{e}^{\mathrm{i}2\omega\tau_0} \end{pmatrix} \bar{z}^2 + \cdots$$

Noticing $G(z,\bar{z}) = \bar{D}[\bar{p}_0 F_1(x_{2,t}(-1)) + F_2(x_{1,t}(-1))]$, we obtain

$$g_{20} = 2\bar{D}(a_2 + b_2\bar{p}_0^3)\mathrm{e}^{-\mathrm{i}2\omega\tau_0},$$

$$g_{11} = 2\bar{D}(a_2 + b_2 p_0\bar{p}_0^2),$$

$$g_{02} = 2\bar{D}(a_2 + b_2 p_0^2\bar{p}_0)\mathrm{e}^{\mathrm{i}2\omega\tau_0},$$

$$g_{21} = 2\bar{D}\{[2W_{11}^{(2)}(-1)b_2\bar{p}_0^2 + 2W_{11}^{(1)}(-1)a_2 + 3b_3 p_0\bar{p}_0^3 + 3a_3]\mathrm{e}^{-\mathrm{i}\omega\tau_0} + [W_{20}^{(2)}(-1)b_2 p_0\bar{p}_0 + W_{20}^{(1)}(-1)a_2]\mathrm{e}^{\mathrm{i}\omega\tau_0}\}.$$

Next, we compute W_{11} and W_{20}. Substituting W, H and (5.33) into equation (5.35) and comparing coefficients, we obtain

$$AW_{20}(\vartheta) = \mathrm{i}2\omega\tau_0 W_{20}(\vartheta) - H_{20}(\vartheta), \qquad AW_{11}(\vartheta) = -H_{11}(\vartheta). \tag{5.36}$$

It is clear that

$$H(z,\bar{z},\vartheta) = \begin{cases} -G(z,\bar{z})q(\vartheta) - \bar{G}(z,\bar{z})\bar{q}(\vartheta) & \text{if } \vartheta \in [-1,0); \\ -G(z,\bar{z})q(0) - \bar{G}(z,\bar{z})\bar{q}(0) + F_0(z,\bar{z}) & \text{if } \vartheta = 0. \end{cases}$$

This yields

$$H_{20}(\vartheta) = -g_{20}q(\vartheta) - \bar{g}_{02}\bar{q}(\vartheta), \qquad H_{11}(\vartheta) = -g_{11}q(\vartheta) - \bar{g}_{11}\bar{q}(\vartheta),$$

$$H_{20}(0) = -g_{20}q(0) - \bar{g}_{02}\bar{q}(0) + \begin{pmatrix} 2b_2\bar{p}_0^2\mathrm{e}^{-\mathrm{i}2\omega\tau_0} \\ 2a_2\mathrm{e}^{-\mathrm{i}2\omega\tau_0} \end{pmatrix},$$

$$H_{11}(0) = -g_{11}q(0) - \bar{g}_{11}\bar{q}(0) + \begin{pmatrix} 2b_2 p_0\bar{p}_0 \\ 2a_2 \end{pmatrix}.$$

On the interval $\vartheta \in [-1,0)$, equation $\dot{W} = AW$ holds and substituting into (5.36) gives rise to

$$\begin{aligned} \dot{W}_{20}(\vartheta) &= \mathrm{i}2\omega\tau_0 W_{20}(\vartheta) + g_{20}q(\vartheta) + \bar{g}_{02}\bar{q}(\vartheta), \\ \dot{W}_{11}(\vartheta) &= g_{11}q(\vartheta) + \bar{g}_{11}\bar{q}(\vartheta) \end{aligned} \tag{5.37}$$

with the initial condition at $\vartheta = 0$ defined by the definition of A:

$$\int_{-1}^{0}[\mathrm{d}\eta(\vartheta)]W_{20}(\vartheta) = \mathrm{i}2\omega\tau_0 W_{20}(0) - H_{20}(0), \qquad \int_{-1}^{0}[\mathrm{d}\eta(\vartheta)]W_{11}(\vartheta) = -H_{11}(0).$$

Solving equations (5.37), we obtain

$$W_{20}(\vartheta) = \frac{\mathrm{i}g_{20}q(0)}{\omega\tau_0}\mathrm{e}^{\mathrm{i}\omega\tau_0\vartheta} + \frac{\mathrm{i}\bar{g}_{02}\bar{q}(0)}{3\omega\tau_0}\mathrm{e}^{-\mathrm{i}\omega\tau_0\vartheta} + E_1\mathrm{e}^{\mathrm{i}2\omega\tau_0\vartheta}, \tag{5.38}$$

$$W_{11}(\vartheta) = -\frac{\mathrm{i}g_{11}q(0)}{\omega\tau_0}\mathrm{e}^{\mathrm{i}\omega\tau_0\vartheta} + \frac{\mathrm{i}\bar{g}_{11}\bar{q}(0)}{\omega\tau_0}\mathrm{e}^{-\mathrm{i}\omega\tau_0\vartheta} + E_2. \tag{5.39}$$

Subject to the initial condition and using equations (5.32), we obtain

$$\left(\mathrm{i}2\omega\tau_0 I_{2\times 2} - \int_{-1}^{0}[\mathrm{d}\eta(\vartheta)\mathrm{e}^{\mathrm{i}2\omega\tau_0\vartheta}]\right)E_1 = \begin{pmatrix} 2b_2\bar{p}_0^2\mathrm{e}^{-\mathrm{i}2\omega\tau_0} \\ 2a_2\mathrm{e}^{-\mathrm{i}2\omega\tau_0} \end{pmatrix},$$

$$\left(\int_{-1}^{0}[\mathrm{d}\eta(\vartheta)]\right)E_2 = \begin{pmatrix} -2b_2 p_0\bar{p}_0 \\ -2a_2 \end{pmatrix}.$$

It follows that

$$E_1 = \frac{2e^{-i2\omega\tau_0}}{D_1\tau_0}\begin{pmatrix} b_2\bar{p}_0^2(\alpha+i2\omega)+a_2\tilde{\mu}e^{-i2\omega\tau_0} \\ b_2\bar{p}_0^2\mu e^{-i2\omega\tau_0}+a_2(\alpha+i2\omega)\end{pmatrix},$$

$$E_2 = \frac{2}{\tau_0(\alpha^2-\tilde{\mu}\mu)}\begin{pmatrix} -\alpha b_2 p_0\bar{p}_0+a_2\tilde{\mu} \\ b_2\mu p_0\bar{p}_0-\alpha a_2\end{pmatrix},$$

where $D_1 = (\alpha+i2\omega)^2-\tilde{\mu}\mu e^{-i4\omega\tau_0}$.

Substituting E_1, E_2 into equations (5.38) and (5.39), we can determine $W_{20}(-1)$, $W_{11}(-1)$, and furthermore, determine g_{21}. Thus, we can compute the following quantities:

$$C_1(0) = \frac{i}{2\tau_0\omega}\left(g_{11}g_{20}-2|g_{11}|^2-\frac{|g_{02}|^2}{3}\right)+\frac{g_{21}}{2},$$

$$T_2 = \frac{1}{\tau_0\omega}\left[-\mathrm{Im}\{C_1(0)\}+\frac{\mathrm{Im}\{\lambda'(\tau_0)\}}{\mathrm{Re}\{\lambda'(\tau_0)\}}\mathrm{Re}\{C_1(0)\}\right].$$

These quantities determine the bifurcated periodic solutions on the centre manifold at the critical value τ_0, concluded by theorem 5.1. Simplifying by a near-identity transformation, we obtain the normal form

$$\dot{z} = i\omega\tau_0 z+\tfrac{1}{2}C_1(0)z|z|^2.$$

Expressed in polar coordinate $z = re^{i\xi}$, this degenerate system becomes

$$\dot{r} = \tfrac{1}{2}\mathrm{Re}\{C_1(0)\}r^3, \qquad \dot{\xi} = \omega\tau_0+\tfrac{1}{2}\mathrm{Im}\{C_1(0)\}r^2 \tag{5.40}$$

and its unfolding is

$$\begin{aligned}\dot{r} &= \nu r+\tfrac{1}{2}\mathrm{Re}\{C_1(0)\}r^3,\\ \dot{\xi} &= \omega\tau_0+\tfrac{1}{2}\mathrm{Im}\{C_1(0)\}r^2.\end{aligned} \tag{5.41}$$

Here ν is an unfolding parameter, whose role is that all possible behaviours of system close to (5.40) must be contained in a system of the form of (5.41).

Theorem 5.1. *If parameters satisfy $\mu\tilde{\mu} < -\alpha^2$, system (2.3) at equilibria E_4, E_5, E_6 and E_7 undergoes a Hopf bifurcation when $\tau = \tau_j$ with $j = 0, 1, \ldots$. The sign of $\mathrm{Re}\{\lambda'(\tau_0)\}\mathrm{Re}\{C_1(0)\}$ determines the direction of the Hopf bifurcation: the Hopf bifurcation is supercritical (subcritical) if $\mathrm{Re}\{\lambda'(\tau_0)\}\mathrm{Re}\{C_1(0)\} < 0$ (> 0) and bifurcated periodic solutions exist for $\tau > \tau_0$ ($< \tau_0$). The sign of $\mathrm{Re}\{C_1(0)\}$ determines the stability of the bifurcated periodic solutions: the periodic solutions are orbitally stable (unstable) if $\mathrm{Re}\{C_1(0)\} < 0$ (> 0). T_2 determines the period of the bifurcated periodic solutions: the period increases (decreases) if $T_2 < 0$ (> 0).*

6. Simulation results: bifurcation of periodic solutions and global gluing bifurcation to butterflies

In this section, we present some detailed simulation results for system (2.3) with parameters $\alpha = 1$, $\beta_1 = 10$, $\beta_2 = 10$, $k = -1$, $h = 0.5$, which give rise to eleven equilibria lying in the region (d) of Figure 4. We focus mainly on the effect of increasing the delay on local dynamical behaviours around equilibria E_4, E_5, E_6, E_7 and on patterns of global continuation of periodic solutions bifurcated from these equilibria.

Equilibrium E_4 is given by $(\tilde{x}, \tilde{y}) = (0.1091, 0.4777)$, and equilibrium $E_5(\tilde{y}, \tilde{x})$ is symmetric to E_4 with respect to the line $y = x$. At E_4, $\mu = f'(\tilde{x}) = 3.4237$ and

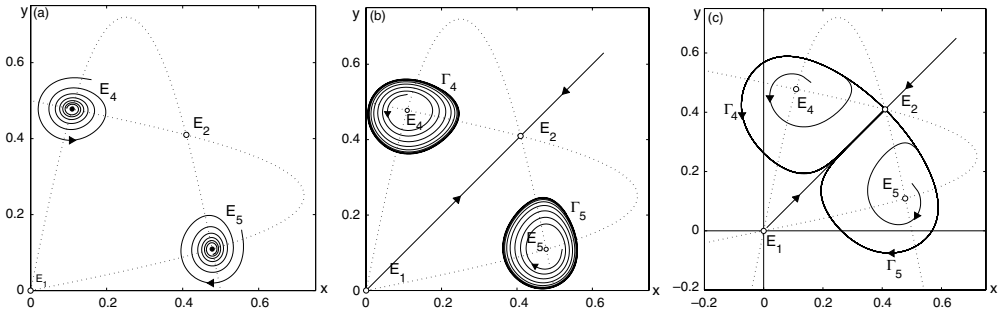

Figure 9. The effect of increasing time delay τ on the local behaviours near E_4 and E_5 and the global pattern of periodic solutions bifurcated from E_4 and E_5 for system (2.3) in the projected (x, y)-plane when $\alpha = 1$, $\beta_1 = 10$, $\beta_2 = 10$, $k = -1$, $h = 0.5$: equilibria E_4 and E_5 are asymptotically stable when $\mu\tilde{\mu} < -\alpha^2$ and $\tau < \tau_0 = 0.0629$, shown in (a); when $\tau > \tau_0$, these equilibria lose their stability and stable limit cycles Γ_4 and Γ_5 appear, shown in (b). (c) shows the butterfly configuration generated in a global gluing bifurcation process as τ increases to the critical value ($\tau = 0.154$): two periodic orbits Γ_4 and Γ_5 are glued together at the saddle point E_2 to form two homoclinic orbits.

$\tilde{\mu} = f'(\tilde{y}) = -4.8376$, which satisfy $\mu\tilde{\mu} < -\alpha^2$. Theorem 4.11 gives the Hopf bifurcation values $\omega = 3.9449$ and $\tau_0 = 0.0629$. Following the computational process in Section 5, we obtain the two important quantities: $C_1(0) = -3.1542 - 7.6011\mathrm{i}$ and $\lambda'(\tau_0) = 13.0615 - 6.7620\mathrm{i}$. Theorem 5.1 concludes that the Hopf bifurcation is supercritical when $\tau = \tau_0$ since $\mathrm{Re}\{\lambda'(\tau_0)\}\mathrm{Re}\{C_1(0)\} < 0$. Four equilibria are asymptotically stable when $\tau < \tau_0$; they become unstable and periodic solutions are bifurcated when $\tau > \tau_0$. Bifurcated periodic solutions are stable since $\mathrm{Re}\{C_1(0)\} < 0$ and the period of the bifurcated periodic solutions decreases initially near τ_0 because $T_2 > 0$.

System (2.3) possesses multiple steady states, including five saddle points and six stable equilibria, and six heteroclinic orbits connecting these steady states. When τ passes the critical value τ_0, the four equilibria E_4, E_5, E_6 and E_7 lose their stability and a Hopf bifurcation takes place at each of these equilibria. These four branches of periodic solutions enjoy the apparent symmetry along the diagonals $|y| = |x|$. To visualize phase-space trajectories for delay differential equations (2.3), we project the trajectories in the infinitely dimensional phase space C into the two-dimensional (x, y)-plane.

Figures 9, 11 and 12 illustrate the effect of increasing time delay τ on the local dynamical behaviours (see figures 9(a) and (b)) near the equilibria E_4 and E_5 and the global patterns of bifurcated periodic solutions of system (2.3). Figure 9(a) with $\tau < \tau_0$ shows the asymptotic and attractive property of equilibria E_4 and E_5. When $\tau > \tau_0$, equilibria E_4 and E_5 lose their stability, a supercritical Hopf bifurcation occurs, and two periodic orbits Γ_4 (anticlockwise) and Γ_5 (clockwise) are generated simultaneously, shown in figure 9(b). Periodic orbits Γ_4 and Γ_5 possess a reflection symmetry with respect to the heteroclinic orbit E_1E_2, which is a segment on the line $y = x$ in the projected (x, y)-plane.

As time delay increases, periodic orbits Γ_4 and Γ_5 on both sides of the heteroclinic orbit E_1E_2 grow and approach the saddle separatrix of E_2. As time delay reaches another critical value ($\tau = 0.154$), periodic orbits Γ_4 and Γ_5 living on the opposite sides of the heteroclinic orbit E_1E_2 are glued together at the saddle point E_2 to form two homoclinic orbits and then are merged into a large periodic orbit $\Gamma_{4,5}$ through the process of a global *gluing bifurcation*, as shown in figure 9(c). Due to the reflection symmetry, homoclinic orbits simultaneously appear on both sides of the heteroclinic orbit and the global pattern of hybrid structure forms

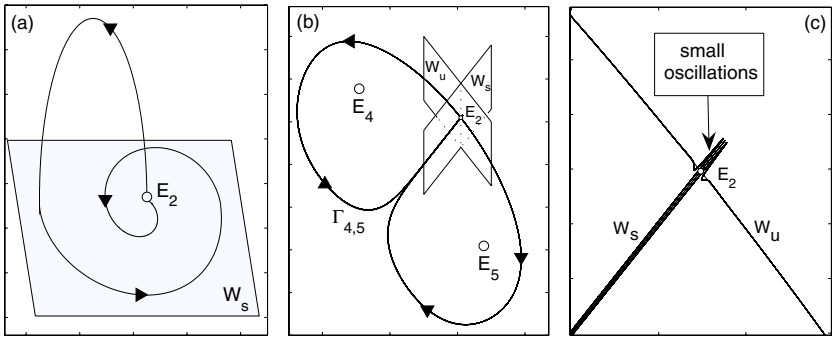

Figure 10. (*a*) An orbit homoclinic to the saddle-focus E_2; (*b*) butterfly configuration generated by a gluing bifurcation at the saddle point E_2; (*c*) zoomed picture around the saddle point E_2 of (*b*): small oscillations appear in the stable manifold of the saddle point E_2. Here, W_s is the infinite-dimensional stable manifold of the saddle-focus E_2 and W_u is the one-dimensional unstable manifold.

a butterfly configuration. The gluing bifurcation has a codimension of one, since only one parameter (time delay) is required to control the homoclinic connection of two periodic orbits.

The homoclinic orbits are given by the intersection of the stable and unstable manifolds of the saddle point E_2. The stable manifold is defined as the set of all trajectories that tend to the saddle point in forward time, and the unstable manifold is defined as the set of all trajectories that tend to the saddle point in backward time. The homoclinic orbits provide a recurrent mechanism in a global setting while the saddle point provides stretching, folding and contraction of the semiflow at the local level.

We now study the stable and unstable manifolds of the saddle point E_2. As time delay reaches the gluing bifurcation point ($\tau = 0.154$), the linearized system of (2.3) has a positive real eigenvalue λ_0 at the saddle point E_2 and infinitely many complex eigenvalues with negative real parts, among which a pair of eigenvalues with the largest real part is $-\lambda_1 \pm i\omega_1$ with $\lambda_1, \omega_1 > 0$. The saddle point E_2 therefore has a one-dimensional unstable manifold, denoted by $W_u(E_2)$, and an infinite-dimensional stable manifold, denoted by $W_s(E_2)$. With parameters $\alpha = 1$, $\beta_1 = 10$, $\beta_2 = 10$, $k = -1$, $h = 0.5$, the three important eigenvalues are $\lambda_0 = 1.8726$, $-\lambda_1 \pm i\omega_1 = -4.7417 \pm i7.0201$ when $\tau = 0.154$.

With a one-dimensional unstable manifold $W_u(E_2)$ and an infinite-dimensional stable manifold $W_s(E_2)$, equilibrium E_2 is of saddle-focus type. An orbit homoclinic to the saddle-focus is depicted in figure 10(*a*). A trajectory spirals close to the stable manifold $W_s(E_2)$ towards the saddle-focus E_2 and is then ejected along the unstable manifold $W_u(E_2)$ to form a global pattern of recurrence. How a periodic orbit (Γ_4 or Γ_5) approaches the homoclinic orbit is determined by the ratio δ of the stable and unstable eigenvalues $\delta = \lambda_1/\lambda_0$ [44]. When $1/2 < \delta < 1$, a homoclinic orbit arises in a sequence of periodic orbits and period-doubling cascades. When $\delta > 1$, a homoclinic orbit arises in a gluing process and the period of the periodic orbit near the homoclinic orbit increases monotonically towards infinity until the bifurcation point is reached. For both cases, the periodic orbits near the homoclinic orbit are stable. However, when $\delta < 1/2$, the periodic orbits are unstable and therefore cannot be observed numerically.

With the above parameters in the gluing process, we have $\delta = 2.532 > 1$ and it indicates the occurrence of a gluing bifurcation. Figure 10(*b*) shows the butterfly configuration in the stable manifold $W_s(E_2)$ and unstable manifold $W_u(E_2)$. Periodic orbits on both sides of the stable manifold $W_s(E_2)$ approach the saddle point E_2 in the same direction and form

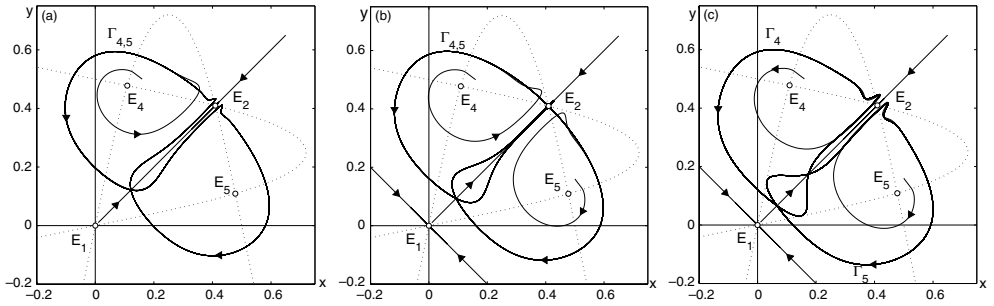

Figure 11. Continuation of global patterns when τ passes the first gluing bifurcation point. (a) shows the glued large periodic orbit $\Gamma_{4,5}$ which has the reflection symmetry with respect to the heteroclinic orbit E_1E_2 in the projected (x, y)-plane. As the time delay increases, the closest distance between the projected trajectory and the saddle point E_2 first increases and then decreases. (b) shows an inverse gluing bifurcation as time delay reaches a critical value ($\tau = 0.21$): the large periodic orbit $\Gamma_{4,5}$ is decomposed into two homoclinic orbits. As time delay passes this inverse gluing bifurcation point, two periodic orbits Γ_4 and Γ_5 emerge, but now each of these periodic orbits crosses transversally the heteroclinic orbit E_1E_2 twice, as shown in (c).

two homoclinic orbits. In a three-dimensional system with a reflection symmetry, a gluing bifurcation can occur in one of three configurations: figure-of-eight, butterfly configuration and spiral configuration. It seems to be the first time we observe a gluing bifurcation which possesses both the spiral configuration and the butterfly configuration (in the projected (x, y)-plane). In the stable manifold $W_s(E_2)$, periodic orbits Γ_4 and Γ_5 when τ is close to 0.154 or the homoclinic orbits when $\tau = 0.154$ exhibit small amplitude oscillations, as shown in figure 10(c).

The number of times when a periodic orbit (Γ_4, or Γ_5, or $\Gamma_{4,5}$) crosses transversally the heteroclinic orbit E_1E_2 seems to be very important. Before the gluing bifurcation point, either Γ_4 or Γ_5 stays on one side of E_1E_2. After τ passes the gluing bifurcation point, as shown in figure 11(a), two homoclinic orbits are destroyed and a large periodic orbit $\Gamma_{4,5}$ emerges. This periodic orbit has the reflection symmetry with respect to the heteroclinic orbit E_1E_2 and crosses transversally E_1E_2 twice. Starting from an initial condition close to the steady state E_4, the projected trajectory is first expelled from one side of the stable manifold $W_s(E_2)$, then makes a long excursion encircling the steady state E_4, and (after crossing transversally the heteroclinic orbit E_1E_2) reaches the opposite side of the stable manifold $W_s(E_2)$ and moves close to the saddle E_2 until it is expelled from the saddle point, completes a long excursion encircling the steady state E_5 and crosses the heteroclinic orbit E_1E_2, finally moves close to the stable manifold $W_s(E_2)$ and completes a cycle. The closest distance between the projected trajectory and the saddle point E_2 increases as time delay increases until time delay reaches the next critical value ($\tau = 0.189\,35$).

Meanwhile, the saddle point E_1 has a positive real eigenvalue λ_0' and infinitely many complex eigenvalues with negative real parts, among which a pair of eigenvalues with the largest real part is $-\lambda_1' \pm \mathrm{i}\omega_1'$. This saddle E_1 has a one-dimensional unstable manifold, denoted by $W_u(E_1)$, and an infinite-dimensional stable manifold, denoted by $W_s(E_1)$. As time delay increases, the periodic orbit $\Gamma_{4,5}$ gets close to E_1 and starts to oscillate along the unstable manifold $W_u(E_1)$. When $\tau = 0.189\,35$, three important eigenvalues of the saddle point E_1 are $\lambda_0' = 2.2325$ and $-\lambda_1' \pm i\omega_1' = -2.2327 \pm \mathrm{i}7.4271$, and hence $\delta' = \lambda_1'/\lambda_0' \simeq 1$. At the same time, the ratio δ of the saddle E_2 decreases to $\delta = 1.8057 > 1$. As τ passes through $\tau = 0.189\,35$, the closest distance between the projected trajectory and the saddle

point E_2 decreases until the time delay reaches the next critical value ($\tau = 0.21$), where a new phenomenon takes place.

When τ is getting close to 0.21, we observe an inverse process of a gluing bifurcation: two portions of the projected trajectory $\Gamma_{4,5}$ close to the stable manifold $W_s(E_2)$ approach the separatrix of the saddle point E_2, and simultaneously generate two homoclinic orbits crossing the heteroclinic orbit E_1E_2. It is natural to call this bifurcation an *inverse gluing bifurcation*. In the inverse gluing bifurcation process, the period of the periodic orbit $\Gamma_{4,5}$ increases monotonically towards infinity until the inverse gluing bifurcation point $\tau = 0.21$ is reached. After time delay passes this bifurcation point, the periodic orbit $\Gamma_{4,5}$ is decomposed into two periodic orbits Γ_4 and Γ_5, as shown in figure 11(c). Each periodic orbit crosses the heteroclinic orbit E_1E_2 twice.

When time delay continues to increase, a sequence of gluing bifurcations and inverse gluing bifurcations occur. Figure 12(a) shows a gluing bifurcation occurring at $\tau = 0.265$. The corresponding homoclinic orbits cross E_1E_2 twice, and the merged periodic orbit when τ passes 0.265 crosses E_1E_2 six times. Figure 12(b) shows an inverse gluing bifurcation occurring at $\tau = 0.295$ and when τ passes 0.295, two periodic orbits (decomposed from the large periodic orbit before its degeneration into two homoclinic orbits) emerge and each crosses E_1E_2 four times.

Meanwhile, due to the reflection symmetry about the stable manifold $W_s(E_1)$, which is a segment on the line $y = -x$ in the projected (x, y)-plane, a similar global bifurcation process occurs in parallel in the opposite side of the stable manifold of $W_s(E_1)$. In a gluing bifurcation process, the periodic orbits Γ_6 and Γ_7 are glued together into a large periodic orbit $\Gamma_{6,7}$ while in an inverse gluing bifurcation process, the periodic orbit $\Gamma_{6,7}$ is separated into two periodic orbits Γ_6 and Γ_7.

When time delay increases to the critical value 0.315, two large periodic orbits $\Gamma_{4,5}$ and $\Gamma_{6,7}$ approach the saddle point E_1 along its saddle separatrix and form two homoclinic orbits to the saddle point E_1 through a gluing bifurcation process. In the gluing process, two butterfly configurations are merged together to form a complex global pattern, as shown in figure 12(c). Such a periodic orbit $\Gamma_{4,5,6,7}$ exhibits small oscillations along the heteroclinic orbits E_1E_2 and E_1E_3. As time delay passes the gluing bifurcation point, the glued larger periodic orbit $\Gamma_{4,5,6,7}$ crosses the heteroclinic orbits E_1E_8 and E_1E_9, and exhibits more and more oscillatory behaviours around three saddle points (E_1, E_2, E_3) and we eventually see a global structure in figure 12(d).

Information of the period of the periodic orbit Γ_4 or $\Gamma_{4,5}$ is summarized in figure 13, when time delay is varied. The segment from A to C corresponds to the process depicted in figures 9(b) and (c). After the local Hopf bifurcation occurs, the period of the periodic orbit Γ_4 first decreases, corresponding to the segment from A to B. However, as Γ_4 moves close to the stable manifold of the saddle point E_2, the period of this periodic orbit starts to monotonically increase and grows to infinity as the gluing bifurcation point is reached at D. The segment from E to G corresponds to the process illustrated in figure 9(c) and figures 11(a) and (b). The period of the glued periodic orbit $\Gamma_{4,5}$ first decreases and then increases to infinity when the inverse gluing bifurcation point is reached at H. Except near a neighbourhood of the bifurcation points (both the gluing bifurcation point and the inverse gluing bifurcation point), the period of the glued periodic orbit $\Gamma_{4,5}$ when τ is between E and G is always greater than the period of the periodic orbit Γ_4 when τ is between A and C. The segment from I to K corresponds to the process described in figures 11(b) and (c) and figure 12(a), and the segment from M to O corresponds to the process described in figures 12(a) and (b). The gluing bifurcation occurs at L and the inverse gluing bifurcation occurs at P. The period of the periodic orbit Γ_4 from I to K and the period of the periodic orbit $\Gamma_{4,5}$ from M to O always decrease first and then increase to infinity.

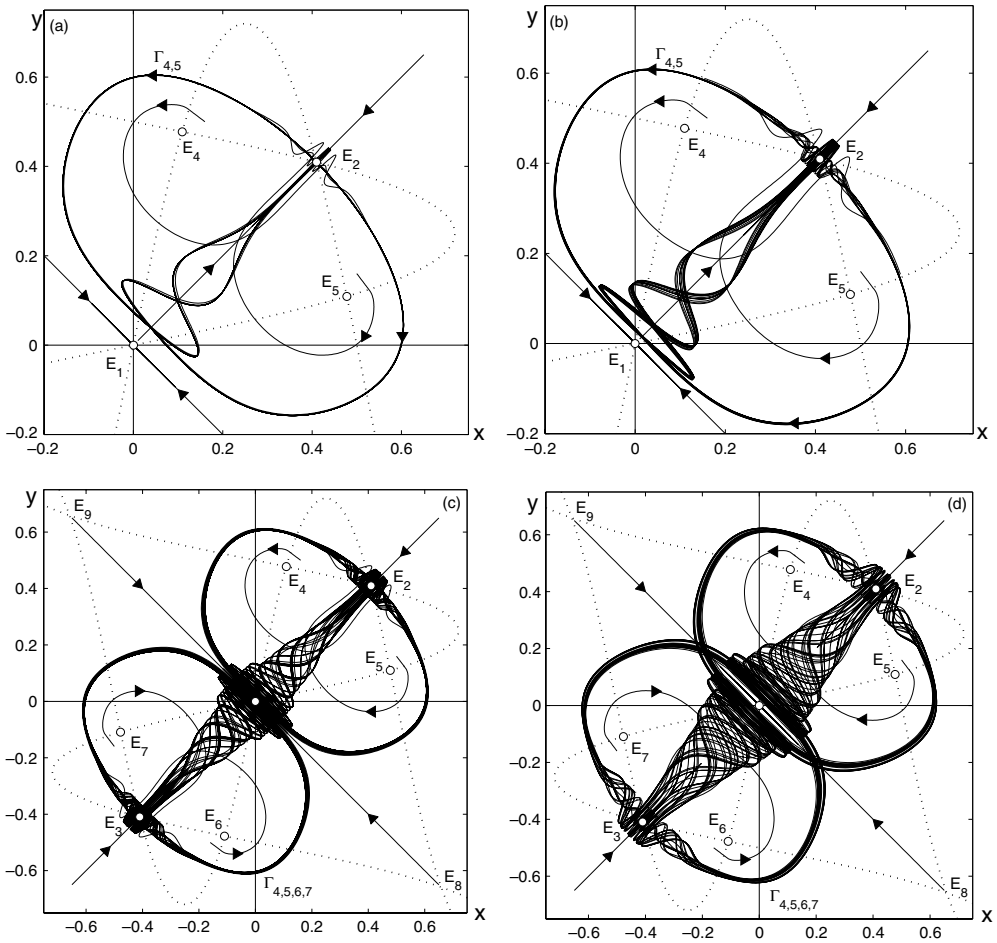

Figure 12. Continuation of global patterns when τ is further increased. (*a*) A gluing bifurcation occurs at $\tau = 0.265$ with a large periodic orbit crossing E_1E_2 six times. (*b*) An inverse gluing bifurcation occurs at $\tau = 0.295$ when the large periodic orbit is degenerated into two homoclinic orbits, and then two periodic orbits emerge with each crossing E_1E_2 four times. (*c*) As time delay reaches a critical value ($\tau = 0.315$), a gluing bifurcation occurs and the periodic orbits $\Gamma_{4,5}$ and $\Gamma_{6,7}$ are glued together into an even larger periodic orbit $\Gamma_{4,5,6,7}$ and the two butterfly configurations are glued into a more complex global pattern. (*d*) More complex structures are developed as τ is further increased.

7. Discussion

In this paper, we gave a detailed mathematical analysis of the dynamics of system (1.1): structure and stability of equilibria in the case where $\tau = 0$ from the point of view of the pitchfork bifurcation and saddle-node bifurcation; impact of time delay on generation and stability of Hopf bifurcation and global dynamical behaviours due to the interaction among limit cycles and equilibria leading to a butterfly structure through a sequence of gluing bifurcations and inverse gluing bifurcations.

Our focus is on multistability: the coexistence of multiple stable patterns including equilibria and periodic orbits, where each stable equilibrium is identified with a static memory

and stable periodic orbits are associated with temporally patterned spike trains. Our results show that system (1.1) has potentially large capacity to encode information in the form of stable equilibria using instantaneous feedback, and in the form of both stable equilibria and stable periodic orbits using delayed feedback. This improvement of network's capacity for associative memory using a non-monotonic activation function provides great potential for artificial neural network applications in dynamic memory.

Saddle points are useful for the maintenance of working memory at the local level while homoclinic and heteroclinic orbits play an important role in securing coding and communication of both working memory and associative memory at the global level. In either the instantaneous feedback case or the delayed feedback case with a small time delay, six heteroclinic orbits, which are segments on the lines $y = x$ and $y = -x$ in the projected (x, y)-plane, separate the phase space into four regions, where trajectories converge to the respective equilibria. Homoclinic orbits arise from a codimension-one homoclinic bifurcation in which the saddle point experiences homoclinicity at both sides of its separatrix. With the reflection symmetry, the appearance of homoclinic orbits is associated with the occurrence of either a gluing bifurcation or an inverse gluing bifurcation, which results in more and more complex dynamics of system (1.1).

We noted that the number of equilibria is dependent on the ratio of the capacitance to the resistance, the synaptic connection strength and the derivative of the activation function. A small time delay can be considered as being associated with 'local' communication between neurons while a large time delay is associated with long range interactions in polysynaptic loops of neurons or neuron populations [21]. Small delays do not change the stability of equilibria, while large delays may destabilize some of the equilibria, leading to Hopf bifurcations of multiple periodic solutions simultaneously bifurcated from equilibria. Our results show that such long range interactions can induce multiple stable periodic orbits, representing frequent firing of neurons with the frequencies of the oscillations being the 'message' transmitted [18]. Furthermore, increasing the time delay of these long range interactions can merge or decompose periodic orbits through a gluing bifurcation or an inverse gluing bifurcation process.

The delay-induced oscillations with a non-zero frequency due to a Hopf bifurcation are commonly referred to as Type II oscillations [45]. The frequency of the delay-induced oscillations continuously changes as time delay is varied. In the range of time delays between the Hopf bifurcation point and the first gluing bifurcation point, corresponding to the segment from A to C in figure 13, the frequency of the periodic orbit first increases from A to B and then decreases from B to C. However, as the delay reaches the gluing bifurcation point at D in figure 13, the periodic orbit becomes a homoclinic orbit and the frequency of such a recurrent orbit becomes zero, and such an oscillation with zero frequency is normally called a Type I oscillation. In the range of delays between the gluing bifurcation point and the inverse gluing bifurcation point, corresponding to the segment from E to G in figure 13, the frequency of the periodic orbit first increases and then decreases. The delay-induced oscillations change from Type I to Type II and then change back to Type I through an inverse gluing bifurcation process at H. The frequency of the periodic orbit varies similarly in the range of delays from I to K and from M to O. The transition between Type I and Type II oscillations illustrates an interesting influence of time delay on neural network computational performance.

Our simulations demonstrate complicated global dynamical phenomena due to interactions among multiple periodic orbits and equilibria. A butterfly structure in the projected (x, y)-plane is generated via a sequence of gluing and inverse gluing bifurcations when time delay is varied. To our knowledge, the transition between gluing bifurcations and inverse gluing bifurcations has not been reported in the literature for infinite-dimensional systems such as DDEs. Furthermore, we observed a gluing bifurcation with both spiral configuration and

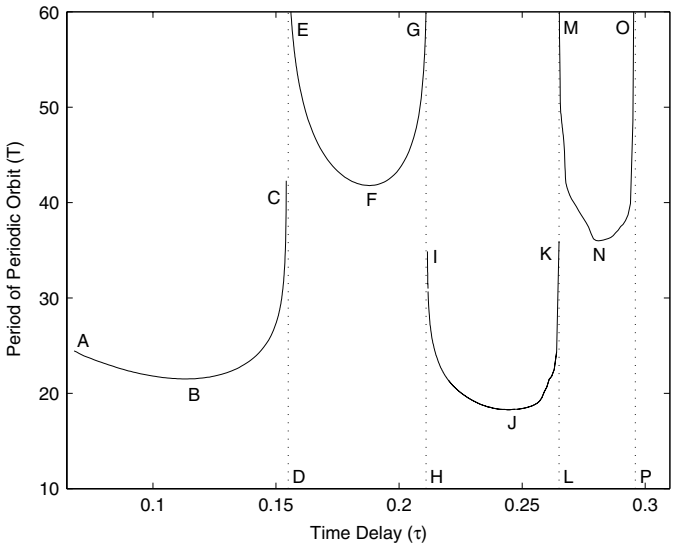

Figure 13. Variation of the period of the periodic orbit Γ_4 or $\Gamma_{4,5}$ as the time delay is varied: the segment from A to C corresponds to the process of figures 9(b) and (c); the segment from E to G corresponds to the process of figure 9(c) and figures 11(a) and (b); the segment from I to K corresponds to the process of figures 11(b) and (c) and figure 12(a); the segment from M to O corresponds to the process of figures 12(a) and (b). The gluing bifurcations occur at D and L, and the inverse gluing bifurcations occur at H and P.

butterfly configuration, a structure that seems to be particular only for very high dimensional dynamical systems. However, an analytic proof and explicit calculation of the critical values of the delay when such gluing and inverse gluing processes occur for system (1.1) remain an open problem for future studies.

Acknowledgments

The authors would like to thank the reviewers for very constructive comments on the manuscript. This research was partially supported by the Canada Research Chairs Program (CRC), by the National Sciences and Engineering Research Council of Canada (NSERC), and by the Mathematics for Information Technology and Complex Systems (MITACS).

References

[1] Anderson J A 1972 A simple neural network generating interactive memory *Math. Biosci.* **14** 197–220
[2] Arbib M A 1998 *The Handbook of Brain Theory and Neural Networks* (Cambridge: MIT Press)
[3] Bélair J and Campbell S A 1994 Stability and bifurcation of equilibria in a multiple-delayed differential equation *SIAM J. Appl. Math.* **54** 1402–24
[4] Bélair J, Campbell S A and van den Driessche P 1996 Frustration, stability, and delay-induced oscillations in a neural network model *SIAM J. Appl. Math.* **56** 245–55
[5] Borisyuk R M and Kirillov A 1992 Bifurcation analysis of a neural network model *Biol. Cybern.* **66** 319–25
[6] Borisyuk G N, Borisyuk R M, Khibnik A I and Roose D 1995 Dynamics and bifurcations of two coupled neural oscillators with different connection types *Bull. Math. Biol.* **57** 809–40
[7] Botelho F 1999 Dynamical features simulated by recurrent neural networks *Neural Netw.* **12** 609–15
[8] Campbell S A, Edwards R and van den Driessche P 2004 Delayed coupling between two neural network loops *SIAM J. Appl. Math.* **65** 316–35

[9] Canavier C, Baxter D, Clark J and Byrne J 1994 Multiple modes of activity in a neuron model suggest a novel mechanism for the effects of neuromodulators *J. Neurophysiol.* **72** 872–82
[10] Chen Y and Wu J 1999 Minimal instability and unstable set of a phase-locked periodic orbit in a delayed neural network *Physica* D **134** 185–99
[11] Chen Y and Wu J 2000 Limiting profiles of periodic solutions of neural networks with synaptic delays *Differential Equations and Computational Simulations* (River Edge, NJ: World Scientific Publishing) pp 55–8
[12] Chen Y and Wu J 2001 Existence and attraction of a phase-locked oscillation in a delayed network of two neurons *Diff. Integral Eqns* **14** 1181–236
[13] Chen Y and Wu J 2001 Slowly oscillating periodic solutions for a delayed frustrated network of two neurons *SIAM J. Appl. Math.* **259** 118–208
[14] Chen Y, Wu J and Krisztin T 2001 Connecting orbits from synchronous periodic solutions in phase-locked periodic solutions in a delay differential system *J. Diff. Eqns* **163** 130–73
[15] Chen Y and Wu J 2001 The asymptotic shapes of periodic solutions of a singular delay differential system (Special issue in celebration of Jack K. Hale's 70th birthday, Part 4 (Atlanta, GA/Lisbon, 1998)) *J. Diff. Eqns* **169** 614–32
[16] Cohen M A and Grossberg S 1983 Absolute stability of global pattern formation and parallel memory storage by competitive neural networks *IEEE Trans. Syst. Man Cybern.* **13** 815–26
[17] Coullet P, Gambaudo J M and Tresser C 1984 Une nouvelle bifurcation de codimension-2: le collage de cycles *C. R. Acad. Sci. Paris* **299** 253–6
[18] Ferster D and Spruston N 1995 Cracking the neuronal code *Science* **270** 756–7
[19] Fiedler B 1988 *Global Bifurcation of Periodic Solutions with Symmetry* (Heidelberg: Springer)
[20] Foss J, Longtin A, Mensour B and Milton J 1996 Multistability and delayed recurrent loops *Phys. Rev. Lett.* **76** 708–11
[21] Foss J, Moss F and Milton J 1997 Noise, multistability, and delayed recurrent loops *Phys. Rev.* E **55** 4536–43
[22] Foss F and Milton J 2000 Multistability in recurrent neural loops arising from delay *J. Neurophysiol.* **84** 975–85
[23] Hassard B D, Kazarinoff N D and Wan Y H 1982 *Theory and Applications of Hopf Bifurcation* (Cambridge: Cambridge University Press)
[24] Herrero R, Farjas J, Pons R, Pi F and Orriols G 1998 Gluing bifurcations in optothermal nonlinear devices *Phys. Rev.* E **57** 5366–77
[25] Herz A V M, Salzer B, Kuhn R and van Hemmen J L 1989 Hebbian learning reconsidered: representation of static and dynamic objects in associative neural nets *Biol. Cybern.* **60** 457–67
[26] Herz A V M 1996 Global analysis of recurrent neural networks *Models of Neural Networks III* ed E Domany *et al* (Berlin: Springer) pp 1–54
[27] Hopfield J J 1982 Neural networks and physical systems with emergent collective computational abilities *Proc. Natl Acad. Sci.* **79** 2554–8
[28] Hopfield J J 1984 Neurons with graded response have collective computational properties like two-state neurons *Proc. Natl Acad. Sci. USA* **81** 3088–92
[29] Hui S and Zak S H 1992 Dynamical analysis of the brain-state-in-a-box neural models *IEEE Trans. Neural Netw.* **1** 86–94
[30] Jin L, Nikiforuk P N and Gupta M M 1994 Absolute stability conditions for discrete-time recurrent neural networks *IEEE Trans. Neural Netw.* **6** 954–63
[31] Kohonen T 1972 Correlations matrix memories *IEEE Trans. Comput.* **C21** 353–9
[32] Kuznetsov Y A 1998 *Elements of Applied Bifurcation Theory* (*Applied Mathematical Sciences* vol 112) (New York: Springer)
[33] Lani-Wayda B 1995 Persistence of Poincaré mappings in functional differential equations (with application to structural stability of complicated behavior) *J. Dyn. Diff. Eqns* **7** 1–71
[34] Lani-Wayda B 1999 Erratic solutions of simple delay equations *Trans. Am. Math. Soc.* **351** 901–45
[35] Ma J and Wu J 2007 Multistability in spiking neuron models of delayed recurrent inhibitory loops *Neural Comput.* **19** 2124–48
[36] Marcus C M and Westervelt R M 1989 Stability of analog network with delay *Phys. Rev.* **39** 347–59
[37] McAuley J D and Stampfli J 1994 Analysis of the effects of noise on a model for the neural mechanism of short-term active memory *Neural Comput.* **6** 668–78
[38] Milton J 2000 Epilepsy: multistability in a dynamic disease *Self-Organized Biological Dynamics and Nonlinear Control* ed J Walleczek (Cambridge: Cambridge University Press)
[39] Morita M, Yoshizawa S and Nakano K 1990 Memory of correlated patterns by associative neural networks with improved dynamics *Proc. INNC'90 (Paris, France)* vol 2 pp 868–71
[40] Morita M 1993 Associative memory with non-monotone dynamics *Neural Netw.* **6** 115–23
[41] Nakano K 1972 Association—a model of associative memory *IEEE Trans. Syst. Man Cybern.* **2** 380–8

[42] Nakahara H and Doya K 1998 Near-saddle-node bifurcation behavior as dynamics in working memory for goal-directed behavior *Neural Comput.* **10** 113–32
[43] Palis J and Taken F 1993 *Hyperbolicity and Sensitive Chaotic Dynamics at Homoclinic Orbits* (Cambridge: Cambridge University Press)
[44] Peacock T and Mullin T 2001 Homoclinic bifurcations in a liquid crystal flow *J. Fluid Mech.* **432** 369–86
[45] Rinzel J and Ermentrout G B 1998 Analysis of neural excitability and oscillations *Methods in Neuronal Modeling: from Ions to Networks* ed C Koch and I Segev (Cambridge, MA: MIT Press)
[46] Sevrani F and Abe K 2000 On the synthesis of brain-state-in-a-box neural models with application to associative memory *Neural Comput.* **12** 451–72
[47] Shayer L P and Campbell S A 2000 Stability, bifurcation, and multistability in a system of two coupled neurons with multiple time delays *SIAM. J. Appl. Math.* **61** 673–700
[48] Shil'nikov L P 1994 Chua's circuit: rigorous results and future problems *Int. J. Bifurcation Chaos Appl. Sci. Eng.* **4** 489–519
[49] Tiňo P, Horne B G, Giles C L and Collingwood P C 1998 Finite state machines and recurrent neural networks—automata and dynamical system approaches *Neural Networks and Pattern Recognition* ed J E Dayhoff and O Omidvar (Orlando, FL: Academic) pp 171–220
[50] Tiňo P, Horne B G and Giles C L 2001 Attractive periodic sets in discrete-time recurrent networks (with emphasis on fixed-point stability and bifurcations in two-neuron networks) *Neural Comput.* **13** 1379–414
[51] Wiggins S 1988 *Global Bifurcations and Chaos* (*Applied Mathematical Sciences* vol 73) (New York: Springer)
[52] Wu J, Faria T and Huang Y S 1999 Synchronization and stable phase-locking in a network of neurons with memory *Math. Comput. Modelling* **30** 117–38
[53] Wu J 2004 *Introduction to Neural Dynamics and Signal Transmission Delay* (Berlin: De-Gruyter)
[54] Wu J and Zhang R Y 2004 A simple delayed neural network for associative memory with large capacity *Discrete Contin. Dyn. Syst.* **4** 853–65
[55] Yoshizawa S, Morita M and Amari S 1993 Capacity of associative memory using a non-monotonic neuron model *Neural Netw.* **6** 167–76
[56] Zhou Z and Wu J 2002 Attractive periodic orbits in nonlinear discrete-time networks with delayed feedback *J. Diff. Eqns Appl.* **8** 467–83